Article

Design and Discovery of N-(2-methyl-5'-morpholino-6'-((tetrahydro-2H-pyran-4-yl)oxy)-[3,3'-bipyridin]-5-yl)-3-(trifluoromethyl)benzamide (RAF709): A potent, selective and efficacious RAF inhibitor targeting RAS mutant cancers

Gisele A. Nishiguchi, Alice Rico, Huw R. Tanner, Robert J. Aversa, Benjamin Robert Taft, Sharadha Subramanian, Lina Setti, Matthew T Burger, Lifeng Wan, Victoriano N. A. Tamez, Aaron Smith, Yan Lou, Paul Andrew Barsanti, Brent A. Appleton, Mulugeta Mamo, Laura Tandeske, Ina Dix, John E. Tellew, Shenlin Huang, Lesley A. Mathews Griner, Vesselina G. Cooke, Anne Van Abbema, Hanne Merritt, Sylvia Ma, Kalyani Gampa, Fei Feng, Jing Yuan, Yingyun Wang, Jacob R Haling, Sepideh Vaziri, Mohammad Hekmat-Nejad, Johanna M. Jansen, Valery R Polyakov, Richard Zang, Vijay Sethuraman, Payman Amiri, Mallika Singh, Emma Lees, Wenlin Shao, Darrin D. Stuart, Michael P Dillon, and Savithri Ramurthy

J. Med. Chem., **Just Accepted Manuscript** • Publication Date (Web): 30 May 2017

	Zang, Richard; Novartis Institute of Biomedical research Sethuraman, Vijay; Novartis, Amiri, Payman; Novartis Institute of Biomedical research Singh, Mallika; Novartis Institute of Biomedical research Lees, Emma; Jounce therapeutics, Inc. Shao, Wenlin; Astra Zeneca, Stuart, Darrin; Novartis Dillon, Michael; Ideaya Biosciences , Ramurthy, Savithri; Novartis Institute of Biomedical research

Design and Discovery of N-(2-methyl-5'-morpholino-6'-((tetrahydro-2H-pyran-4-yl)oxy)-[3,3'-bipyridin]-5-yl)-3-(trifluoromethyl)benzamide (RAF709): A potent, selective and efficacious RAF inhibitor targeting RAS mutant cancers

Gisele A. Nishiguchi[2], Alice Rico[1], Huw Tanner[1], Robert J. Aversa[2], Benjamin R. Taft[1], Sharadha Subramanian[1], Lina Setti[1], Matthew T. Burger[2], Lifeng Wan[1], Victoriano Tamez[2], Aaron Smith[1], Yan Lou[1], Paul A. Barsanti[1], Brent A. Appleton[1], Mulugeta Mamo[1], Laura Tandeske[6], Ina Dix[3], John E. Tellew[4], Shenlin Huang[4], Lesley A. Mathews Griner[5], Vesselina G. Cooke[5], Anne Van Abbema[6], Hanne Merritt[6], Sylvia Ma[6], Kalyani Gampa[5], Fei Feng[5], Jing Yuan[5], Yingyun Wang[6], Jacob R. Haling[4], Sepideh Vaziri[4], Mohammad Hekmat-Nejad[6], Johanna M. Jansen[1], Valery Polyakov[1], Richard Zang[1], Vijay Sethuraman[6], Payman Amiri[6], Mallika Singh[6], Emma Lees[5], Wenlin Shao[5], Darrin D. Stuart[5], Michael P. Dillon[2], Savithri Ramurthy*[1]

1 Global Discovery Chemistry, Novartis Institutes for BioMedical Research, 5300 Chiron Way, Emeryville, California 94608, United States

2 Global Discovery Chemistry, Novartis Institutes for BioMedical Research, 250 Massachusetts Avenue, Cambridge, Massachusetts 02139, United States

3 Global Discovery Chemistry, Novartis Institutes for BioMedical Research, Novartis Pharma AG, Werk Klybeck, Postfach, CH-4002 Basel, Switzerland

4 Genomics Institute of the Novartis Research Foundation, 10675 John Hopkins Dr, San Diego, C California 92121

5 Oncology, Novartis Institutes for BioMedical Research, 250 Massachusetts Avenue, Cambridge, Massachusetts 02139, United States

6 Oncology, Novartis Institutes for BioMedical Research, 5300 Chiron Way, Emeryville, California 94608, United States

ABSTRACT:

RAS oncogenes have been implicated in >30% of human cancers, all representing high unmet medical need. The exquisite dependency on CRAF kinase in KRAS mutant tumors has been established in genetically engineered mouse models and human tumor cells. To date, many small molecule approaches are under investigation to target CRAF, yet kinase-selective and cellular potent inhibitors remain challenging to identify. Herein, we describe **14** (RAF709)[1], a selective B/C RAF inhibitor, which was developed through a hypothesis-driven approach focusing on drug-like properties. A key challenge encountered in the medicinal chemistry campaign was maintaining a balance between good solubility and potent cellular activity (suppression of pMEK and proliferation) in KRAS mutant tumor cell lines. We investigated the small molecule crystal structure of lead molecule **7** and hypothesized that disruption of the crystal packing would improve solubility, which led to a change from N-methylpyridone to a tetrahydropyranyl oxy pyridine derivative. **14** proved to be soluble, kinase selective and efficacious in a KRAS mutant xenograft model.

INTRODUCTION

The mitogen-activated protein kinase (MAPK) signaling pathway plays a major role in the regulation of multiple cellular functions. The pathway is activated through extracellular signals that in turn induce the RAS proteins (K-, N-, HRAS) to exchange GDP for GTP, resulting in activation of the RAF/MEK/ERK cascade. The MAPK pathway is often constitutively activated in human cancers through activating mutations in the RAS proteins or BRAF. In fact, the RAS genes are the most frequently mutated oncogenes in human tumors, however, targeting RAS directly as a cancer therapeutic has been challenging. Recent studies have described approaches to selectively inhibit $KRAS^{G12C}$ through covalent targeting, resulting in a cellular active inhibitor in the low micromolar range. [2-4] While such covalent

inhibitors demonstrate proof-of-concept for targeting $KRAS^{G12C}$-driven tumors, other RAS mutant alleles remain undruggable.

In considering targets downstream of mutant RAS, emerging biology from genetically engineered mouse models and tumor cell lines has begun to uncover which effectors are critical for tumorigenesis, providing new opportunities for therapeutic development. For example, CRAF was shown to be the critical mediator of mutant KRAS-driven cell proliferation and tumor development in both cellular and genetically engineered mouse tumor models.[5,6] CRAF was also shown to play a critical role in feedback-mediated pathway reactivation following MEK inhibitor[7] treatment in KRAS mutant cancers. In addition, CRAF plays an essential role in mediating paradoxical activation following BRAF inhibitor treatment.[8-10] Thus selective inhibitors that potently inhibit the activity of B/CRAF could be both effective in blocking mutant RAS-driven tumorigenesis and preventing feedback mediated reactivation While selective RAF inhibitors such as vemurafenib (**1**) have been developed to treat $BRAF^{V600E}$ mutant tumors, these inhibitors are ineffective against tumors with wild-type BRAF and in fact can accelerate the growth of RAS mutant tumors through paradoxical activation of RAF dimers.[11,12] LY3009120 (**2**) has recently been described as an effective inhibitor of RAF dimers and demonstrates efficacy against some preclinical models of RAS mutant tumors; however, it appears to inhibit several other kinases, including those that have important roles in cancer such as Ephrin receptors, JNK and SRC family members.[13] Thus, a potent inhibitor of RAF dimers with an improved selectivity profile will be invaluable in assessing the therapeutic utility and therapeutic index in RAS mutant tumors.

Chart 1

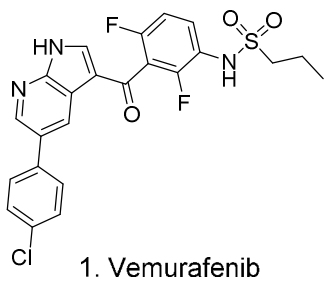

1. Vemurafenib

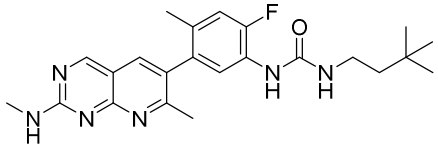

2. LY3009120

RESULTS AND DISCUSSION

The major medicinal chemistry goal of this project was to identify highly selective RAF inhibitors that would potently suppress the RAF-MEK-ERK pathway in KRAS mutant tumor cells without causing paradoxical activation. For this purpose, we developed a full length CRAF biochemical assay as well as Calu-6 ($KRAS^{Q61K}$) cell proliferation and pMEK target modulation assays in which inhibition and activation of the pathway could be measured. Herein we describe our hit finding approach, the design and the synthesis of analogues that led to the discovery of **14 (RAF709)**, a RAF inhibitor that is well-tolerated and efficacious in KRAS mutant xenograft models.

In order to assess whether any existing RAF kinase inhibitor chemotypes were able to suppress pMEK in KRAS mutant tumor cells without inducing paradoxical activation, we pursued an accelerated hit finding strategy that centered on leveraging our existing RAF inhibitor knowledgebase. A dataset from 28k compounds that had shown evidence of RAF inhibition in historical biochemical or cellular assays was assembled. Subsets of this collection were selected for the CRAF biochemical assay and the pMEK target modulation assay in Calu-6 ($KRAS^{Q61K}$) cells. The overarching selection criterion was to ensure sampling of all chemotypes for which there were analogues with good cellular potency in order to ensure we could assess the potential for paradoxical activation. A set of 116 compounds with evidence of pMEK suppression in Calu-6 cells was selected for assessment of paradoxical activation.

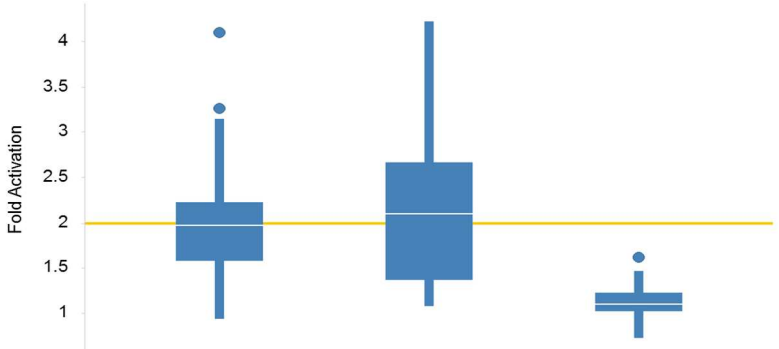

	Type-1 (DFG in, αC-helix in)	Type-1.5 (DFG in, αC-helix out)	Type-2 (DFG out, αC-helix in)
Count	43	27	46
Median	2.0	2.1	1.1

Figure 1. Box-plot of the distribution of fold-activation of pMEK in Calu-6 cells for each of the annotated types (mechanisms) of kinase inhibition [14] based on medicinal chemistry scaffold matches. The 116 compounds in this analysis had a CRAF IC_{50} varying from 42 nM to 30 pM and an EC_{50} in the pMEK target modulation assay in Calu-6 cells < 0.3 μM. The solid line at 2-fold-activation indicates the team's assessment of a relevant cut-off.

From the analysis of this data set, there was a consistent trend towards type 2 inhibitors (DFG out, αC-helix in) exhibiting less paradoxical activation compared to type 1 (DFG in, αC-helix in) and 1.5 (DFG in, αC-helix out)[15,16] modes of inhibition (Figure 1). Compound **1** did not meet the criteria (pMEK >30 μM) to be considered in the data set. On the basis of this observation, the team focused on type 2 inhibitors to further progress towards our medicinal chemistry goal. In depth data mining and further profiling of the hits uncovered several issues associated with type 2 inhibitors, including poor kinase selectivity, low aqueous solubility and high lipophilicity. With these liabilities in mind, we hypothesized that increased levels of saturation could be an approach to improve solubility and enhance kinase selectivity. It has been documented that an increase in the fraction of sp^3 atoms (Fsp^3), defined as the ratio of sp^3 atoms to the total number of non-hydrogen atoms in the molecule, is associated with decrease in melting point and improved solubility for small molecules.[17] At the same time, higher sp^3 character within a given molecule can also offer the opportunity for higher specificity in receptor/ligand complementarity and potentially mitigate off-targets binding.[18] This hypothesis led the team to further probe our type 2 hits leading to the prioritization of compound **3** (Figure 2), a starting point that has measurable solubility and an attractive kinase selectivity profile relative to other hits. In a KINOME*scan*® binding displacement assay,[19, 20] **3** had a selectivity score S(35) of 0.076 when screened at 10 μM, indicative of high kinase selectivity. The morpholine moiety as a potential hinge binder was also viewed as a unique feature within RAF kinase inhibitors.

In order to elucidate the binding mode, we obtained an X-ray co-crystal structure of **3** complexed with the kinase domain BRAF. As illustrated in Figure 2, the oxygen of the morpholine makes a H-bond

interaction to the back-bone NH of residue C532 in the hinge region (O…N distance is approximately 2.7 Å). The pyrimidine core is situated in a hydrophobic region, approximately 3.6 Å away from F595, which could be consistent with an edge to face or T-shaped pi-interaction. The exact type of this interaction is difficult to ascertain due to the 2.4 Å resolution of the crystal structure. Because the two nitrogen atoms of the pyrimidine core are facing the solvent, they are unlikely to adversely affect the potency of the compound, but are beneficial for lowering lipophilicity and probably, enhancing its solubility. The central phenyl is twisted out of the plane of the molecule due to the presence of the 'flag' methyl allowing the amide moiety to engage the protein in two hydrogen bond interactions typical for type 2 inhibitors. The carbonyl makes a H-bond to D594 (O…N distance is approximately 2.7 Å) and the NH is 2.9 Å away from E501 without destroying the salt bridge between K483 and E501. The *t*-butyl phenyl occupies a hydrophobic region referred to here as the induced fit pocket. The protein adopted an inactive conformation characteristic for type 2 inhibitors with the DFG out and the αC-helix in.[21]

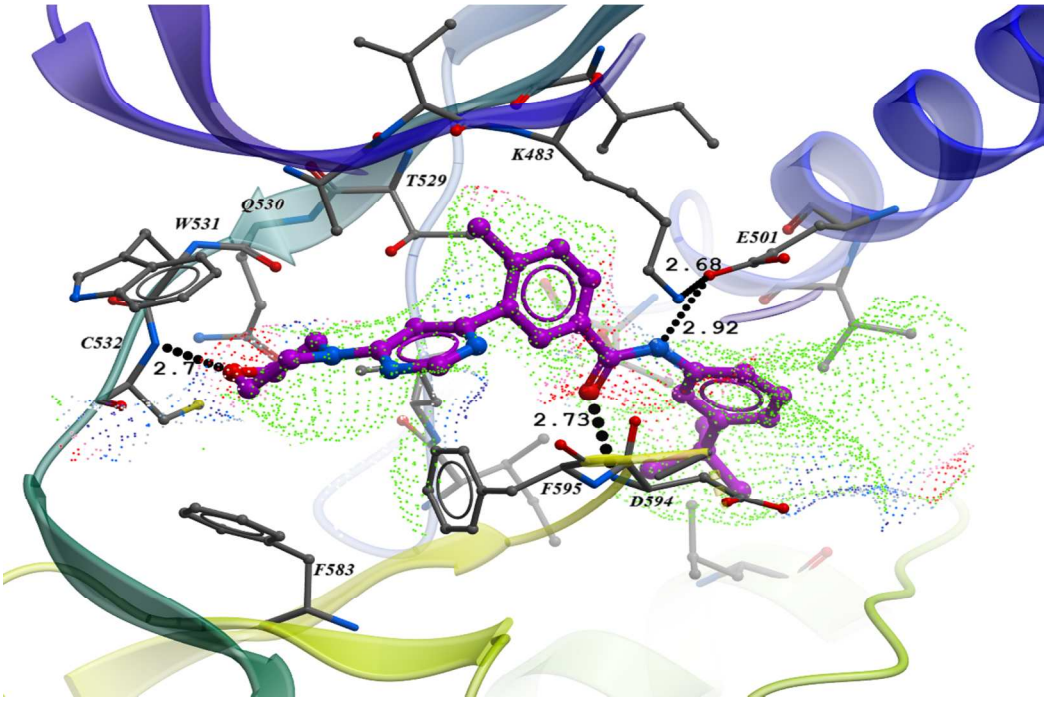

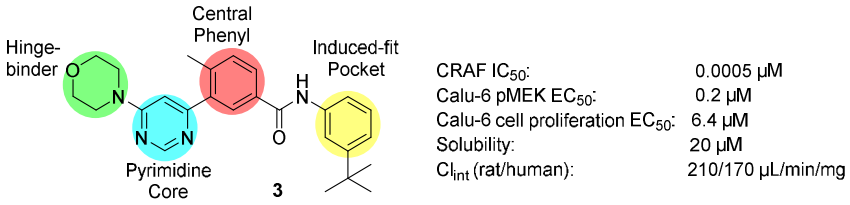

Figure 2. X-ray structure of **3** in the BRAF construct (PDB 5VAL)[22] illustrating key features of protein ligand interactions depiction of the crystalized ligand illustrating most important features of protein ligand interactions, labeled key residues, and a ligand pocket surface. All distances are in Å.

We initiated hit optimization with **3** (Figure 2) aiming to improve the solubility and cellular potency. Through hit expansion from our compound collection we identified analogue **4** (Table 1) with a lower cLogP (4.1) and similar cellular potency as **3**. From this compound, we synthesized the corresponding reverse-amide match **5** (Table 1) in order to assess if there is a favorable amide orientation for the series. Compound **5** had comparable biochemical potency and anti-proliferative effect relative to **4** with improved target modulation, measurable solubility and reasonable clearance (rat and human liver microsomes Cl_{int}: 79 and 43 µL/min/mg) making this a preferred amide isomer for subsequent analogs.

Table 1. Biochemical and cellular activity, permeability and solubility data for compounds 3, 4, 5, and 6

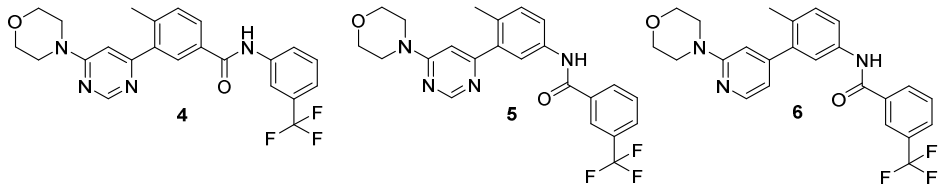

Cmpd	CRAF IC_{50} (µM)	pMEK Calu-6 EC_{50} (µM)	CP Calu-6 EC_{50} (µM)	Caco-2 Papp AB/BA* ($x10^{-6}$ cm/s)	Sol** (µM)	cLogP***
3	0.0005	0.2	6.4	15/15	20	4.7
4	0.002	0.7	3.1	15/8	<2	4.1
5	0.0001	0.08	5.2	19/38	16	4.0

6	0.0002	0.2	0.7	^/1.8	<2	4.5

*Forward and reverse flux were measured via transit across 21-day cultured Caco-2 monolayers at pH7.4 with quantification via LC/MS/MS. **Solubility (shake–flask assay) was measured with Cl-free PBS at pH 6.8. ***cLogP was calculated using Biobyte software. ^Poor recovery.

Based on the BRAF co-crystal structure with **3**, we postulated that removal of the pyrimidine nitrogen adjacent to the central phenyl should not affect biochemical potency since both nitrogens in the pyrimidine ring face the solvent. The pyridine analogue **6** (Table 1) was found to have similar potency as **5** in the biochemical assay. The resulted torsional angle increase between the pyridine ring and the central phenyl ring relative to the pyrimidine-central phenyl ring, led to the hypothesis that there is some flexibility (around the hydrophobic pocket and the gate keeper residue T529) would be tolerated. . While the poor solubility of compound **6** still remained a concern, the potent cellular activity provided confidence in the series and led to the hypothesis that core modifications could be utilized to modulate cell potency as well as the properties of the molecules. This turned our attention to the lipophilicity of the cores and we focused on designing analogues with lower cLogP.

In an effort to decrease the cLogP, we investigated core modifications with more polar heterocycles in conjunction with central and induced fit pyridyl modifications. Four representative examples of our SAR set are illustrated in Table 2. We quickly learned from compounds **7, 8, 9** and **10** (Table 2) that intrinsic clearance and solubility were consistently improved but the increased polarity eroded cellular potency in many cases. We hypothesized that optimal polarity might be essential to balance potency and drug-like properties and strategized that making different core modifications would allow us to find the right balance. The balanced profile of solubility, target modulation and anti-proliferative effect of pyridone **7** led us to select this compound over the other analogues for further profiling. Since kinase selectivity is one of the liabilities with type 2 inhibitors, we screened this compound using the KINOME*scan* binding displacement assay against 456 human kinases and their relevant mutants at 1 μM (Figure 3). Of the 456 kinases tested, it showed a high level of selectivity, demonstrating greater than 99% binding to BRAF,

BRAF^{V600E} and 90% binding to CRAF with binding to only one off-target at >80% (PDGFRβ,89%) and a selectivity score (S-score) of S(35) = 0.015. In cellular target modulation, it was potent and showed minimal paradoxical activation in KRAS mutant cell lines.

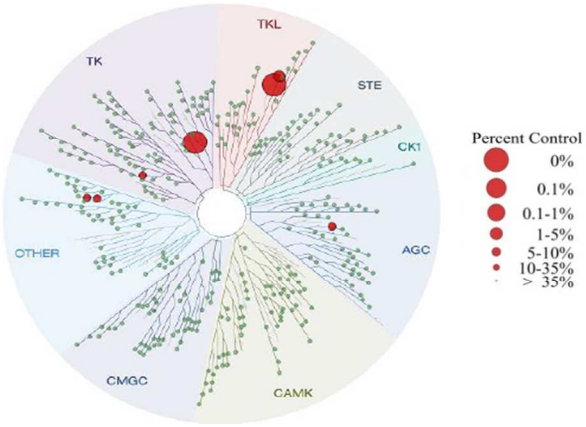

Figure 3. KINOME*scan* profile of **7**

Table 2. Potency, ADME and solubility data for analogues with a lower cLogP

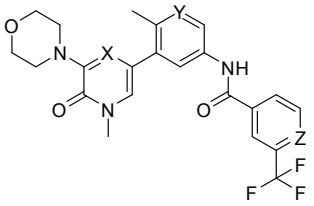

Cmpd	X	Y	Z	CRAF IC_{50} (μM)	pMEK Calu-6 EC_{50} (μM)	CP Calu-6 EC_{50} (μM)	Caco-2 Papp AB/BA ($x10^{-6}$ cm/s)	Clint (human microsomal μL/min/mg)	Sol (μM)	cLogP
7	CH	CH	CH	0.0004	0.076	0.5	20/22	51	70	3.5
8	N	CH	CH	0.0003	0.2	4.1	21/16	110	190	3.2
9	CH	N	CH	0.0008	0.46	1.8	7/43	<7.7	20	2.8

10	CH	N	N	0.001	3.96	>30	3/39	<7.7	1040	1.5

Compound **7** also demonstrated good permeability, minimum efflux based on Caco-2 assays and moderate *in-vitro* clearance measured in rat (Cl_{int}: 46 μL/min/mg) and human liver microsomes (Cl_{int}: 51 μL/min/mg). Given its favorable *in vitro* ADME profile, the pharmacokinetics of **7** was evaluated in rats (Sprague Dawley) at 1 mg/kg *IV* and 3 mg/kg *PO*. The results indicated that **7** had an oral total exposure (AUC) of 0.438 μM*hr, high *in-vivo* clearance (53 mL/min/kg), Cmax of 0.15 μM and low-moderate bioavailability of 22%. Formulating **7** proved challenging, potentially due to its solubility and this hindered further *in-vivo* studies, especially at higher doses where a lack of dose-proportional exposure was observed. More in depth physicochemical characterization of **7** revealed a melting point >230 °C (decomposed) which clearly suggested that tight crystal packing in the solid phase might also have contributed to the poor solubility and this was further supported by measuring the solubility from crystalline material which gave a value of 4 μM. Therefore, lead optimization centered on further addressing the solubility of the series without compromising the cellular potency.

In order to further understand the chemical modifications required to disrupt crystal packing or lowering the melting point we investigated the small molecule X-ray structure of **7**.[22] The molecules are arranged in pairs oriented head-to-tail so that the amide nitrogen of each molecule (N22) forms a moderately strong H-bond to the carbonyl oxygen (O12) of the pyridone ring of the second molecule (Figure 4). The distance between N and O atoms is 2.99 Å. Additionally, the same pyridone rings are oriented in the parallel planes with the distance of 4.21 Å between them which is consistent with the parallel displaced *pi*-interaction.

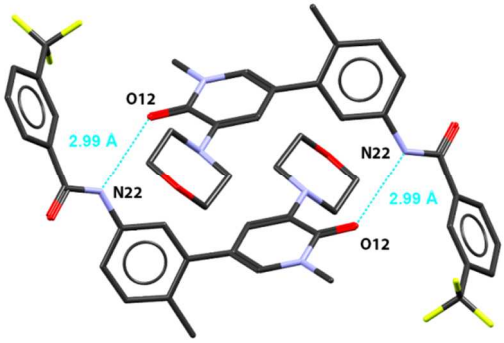

Figure 4. Small molecule X-ray structure of compound **7**.

Based on this analysis we hypothesized that removal of the carbonyl would disrupt the intermolecular hydrogen bond network and furthermore the introduction of sp^3 character in close proximity to the core could potentially disrupt the parallel displaced pi-stacking interaction. To test our hypothesis, the 3-morpholino-2-oxypyridine core emerged as a valuable scaffold (Table 3). In this series, the pyridone carbonyl was replaced by the ether oxygen and the directionality of the methyl provided a solvent exposed vector. This core was initially derived from the pyridone alkylation reaction (Scheme 1) to provide the minor O-alkylated product, exemplified by **11** (Table 3). It is noteworthy to highlight the serendipitous nature of the discovery of the O-alkylated core '*as a reaction by-product'*.

While compound **11** was moderately potent in cellular assays and remained poorly soluble, we hypothesized that the methoxy group was satisfying the disruption of the inter-molecular hydrogen bonding network but was not large enough to disrupt the parallel *pi*-interaction. Given the Fsp^3 of compound **11** is 0.29, we envisioned that an increase in Fsp^3 around the methoxy group might address the solubility liability. As shown in Table 3, by increasing the size of the R_1 substituent from methyl to isopropyl, compound **12** was obtained. Although its solubility was still low, the fact that cell potency was maintained was encouraging and larger substituents were investigated. A glycol moiety **13** (Table 3) was tolerated and it provided a lower cLogP and higher Fsp^3 with solubility trending in a favorable direction at 24 μM, however an efflux liability was introduced. By exploring larger R_1 substituents such as the tetrahydropyran in **14** high throughput solubility was improved to 200 μM and the solubility of the highly

stable crystalline material was measured to be 120 μM (melting point: 196 °C). Moreover, pMEK cellular potency was preserved and low efflux was maintained. Overall, **14** provided the most favorable balance of physicochemical properties and cellular potency and hence it was selected for further profiling.

Table 3. Effect of Increased Fsp^3 on solubility, permeability and activity in the oxy-pyridine core

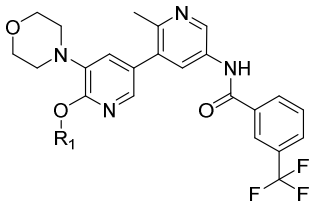

Cmpd	R_1	CRAF IC_{50}(μM)	pMEK Calu-6 EC_{50} (μM)	CP Calu-6 EC_{50}(μM)	Caco-2 Papp AB/BA ($x10^{-6}$ cm/s)	Sol (μM)	cLogP	Fsp^3
11	Me	0.0004	0.25	1.6	16/14	<2	4.6	0.29
12	$-CH_2(CH_3)_2$	0.0006	0.3	2.9	-	<2	5.4	0.35
13	$-CH_2CH_2OH$	0.0005	0.08	2.5	5/45	24	3.7	0.32
14		0.0005	0.02	0.95	15/13	200	4.2	0.39

X-ray structure of 14. The X-ray co-crystal structure of **14** in BRAF illustrated in Figure 5 shows a binding mode similar to **3** with respect to the morpholine and induced fit moiety. The central pyridine occupies the space of the corresponding central toluyl tightly filling up a narrow hydrophobic pocket formed by the sidechains of K483, I527, T529, and A481. The CF_3 phenyl occupies the hydrophobic induced-fit pocket similar to the structure of compound **3**. The tetrahydropyran faces a solvent opening in the ATP binding pocket which can accommodate such a large group. The protein maintains the DFG-out αC-Helix-in inactive conformation consistent with a type 2 mode of inhibition.

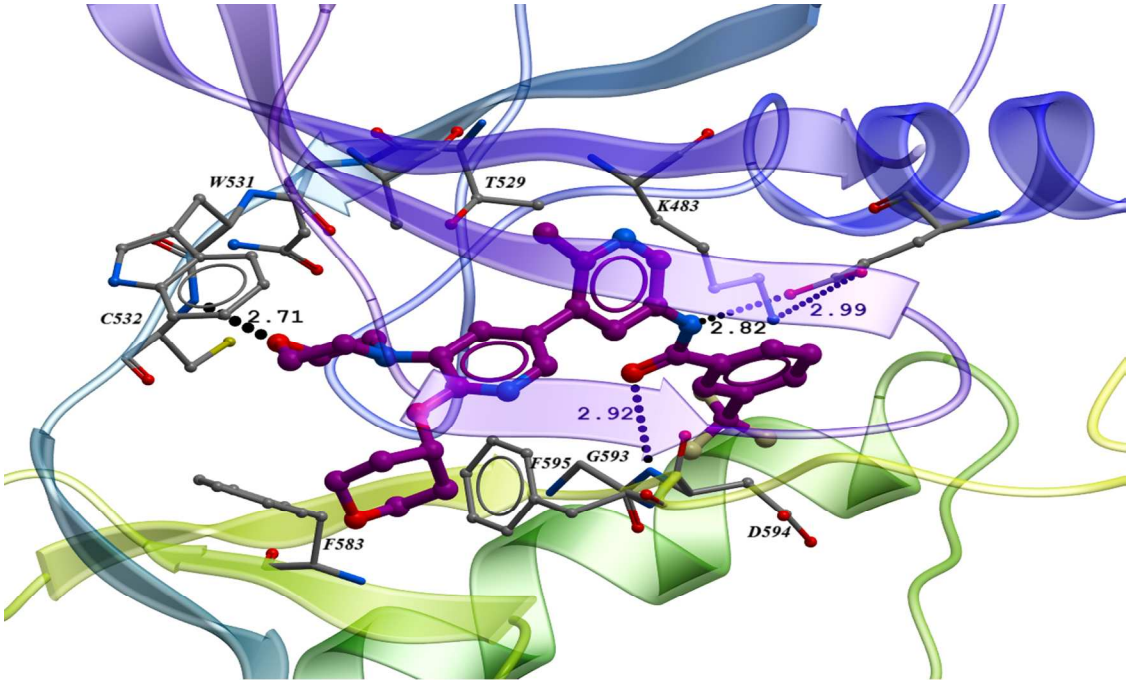

Figure 5: X-ray structure of **14** in BRAF (PDB 5VAM)[22]

***In vitro* profiling of 14[23].** The biochemical activity of **14** was further characterized against purified full-length BRAF where the IC_{50} measured 0.0004 μM which is in-line with the potency against CRAF. Off-rate is an important attribute of potency, impacting both the cellular activity in the face of feedback and the PK/PD relationship *in vivo*. Therefore we attempted to measure the dissociation rate constant for **14** using the rapid dilution method and it appeared to have very slow dissociation kinetics ($T_{1/2}$ > 6.5 hrs). In cellular assays the dose-response of pMEK and pERK were measured in Calu-6 cells with EC_{50} = 0.02 and 0.1 μM with minimal paradoxical activation (Figure 6A) and inhibition of proliferation with EC_{50} = 0.95 μM. Compound **1** clearly demonstrated paradoxical activation in the pMEK assay (Figure 6A) with maximum activity at 3 μM and no resultant inhibition up to the highest concentration tested (30 μM). The ability of **14** to stabilize RAF dimerization was measured using the CRAF:BRAF NanoBiT™ luciferase complementation assay (Promega). Consistent with most other RAF inhibitors, **14** stabilized BRAF-CRAF dimers with an EC_{50} = 0.8 μM (Figure 6B), while **1** demonstrated modest stabilization of dimers in this assay. Additional supporting data was revealed in the X-ray crystal structure of **14** (Figure 5), where

each BRAF protomer in the dimer structure was loaded with compound. This also demonstrated that (at least under the conditions of crystallization), binding of **14** to one protomer did not preclude binding to the other protomer in the dimer structure. Altogether, these data demonstrate that **14** stabilizes RAF dimers but is relatively equipotent at inhibiting both protomers since it induces minimal paradoxical activation but effectively suppresses signaling.

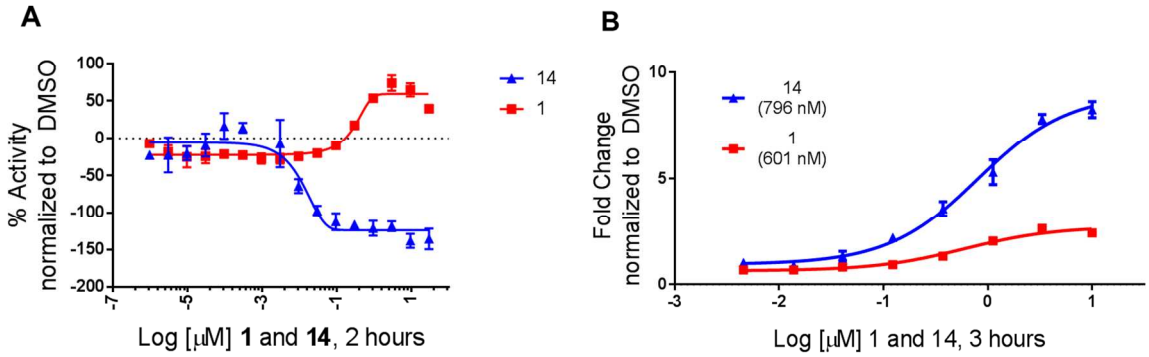

Figure 6. A: pMEK inhibition and activation of **1** and **14** in Calu-6 RAS mutant cells; **B:** Effect of 1 and 14 on the stimulation of dimerization in HCT116 cells.

Kinase Selectivity of 14. Consistent with this chemical series, **14** was found to be highly selective when evaluated using the KINOME*scan*^{Tm} screening platform. Of the 456 kinases tested[19, 20], **14** showed a high level of selectivity, demonstrating greater than 99% on-target binding to BRAF, BRAF^{V600E}, and CRAF at 1 μM and very few off-targets with DDR1 (>99%), DDR2 (86%), FRK (92%), PDGFRb (96%) the only kinases with binding >80% at 1 μM. To the best of our knowledge, this compound exhibits the highest level of kinase selectivity amongst known type 2 RAF inhibitors with a selectivity score of S(35) = 0.018.[20]

Compounds such as **14** and **7** with a morpholine as the hinge binding moiety appeared to be remarkably selective inhibitors of RAF kinases often exhibiting more than 10,000 fold difference in the binding affinities even toward other structurally similar proteins like p38 and EGFR. The combination of a morpholine, a central core attached to the perpendicular central phenyl and an appropriate group to fill the

induced-fit hydrophobic pocket (Figure 5) allowed us to fine-tune inhibitors to accommodate the unique geometries of RAF kinases ensuring sub-optimal binding to other kinases.

Pharmacokinetics of 14. **14** was reasonably stable in plasma after a 3 hour incubation at 37 °C across species [plasma stability (%remaining): rat 85%, mouse 82%, dog 95%, human 101%] and plasma protein binding was measured to be 98% across species. In pharmacokinetic experiments (Table 4), **14** had moderate clearance in mouse (35 ml/min/kg) and dog (14 ml/min/kg) and high clearance in rat (50 ml/min/kg). Cmax in mouse (1 μM), dog (0.5 μM) and rat (0.5 μM) reached pharmacologically active concentrations and, acceptable oral availability was observed in mouse (68%), rat (24%) and dog (48%). Compared to **7**, **14** was less challenging to formulate due to higher intrinsic solubility which enabled progression into PK/PD and efficacy studies at higher doses.

Table 4: PK profile of 14 across species

Species	Dose (*i.v./p.o*, mg/kg)	C_{max} (*p.o.*, μM)	AUC_{inf} (*p.o.*, μM*hr)	Cl (ml/min/kg)	Vss (L/kg)	F(*po)* (%)
Mouse	1 / 3	1.0	1.7	35	1.2	68^
Rat	3 / 10	0.8	1.5	50	3.5	24*
Dog	0.3 / 1	0.5	1.0	14	3.1	48*

*: formulation (*i.v./p.o)*: 20%PEG300 + 5%Solutol ^: formulation (*i.v./p.o)*: 25% PEG300 + 5% Solutol

PK/PD of 14. The PK/PD relationship of **14** was examined in the Calu-6 xenograft model in nude mice. The plasma exposure of **14**, and levels of pERK in tumor tissue were determined following a single oral administration across a dose range of 10, 30 and 200 mg/kg. **14** showed dose-proportional increases in plasma exposure and a corresponding dose-dependent inhibition of pERK in Calu-6 tumors (Figure 7).

At 24 hrs post-dose of 10 mg/kg **14**, plasma levels were below the lower limit of quantitation and there was a complete lack of pERK inhibition. At the highest dose level of 200 mg/kg free plasma concentrations were maintained above the cellular *in vitro* pERK IC_{50} value for the entire 24 hours, which was consistent with sustained inhibition of pERK ≥ 70%. It is interesting to note that at the 10 mg/kg and 30 mg/kg doses, the pathway seemed to be hyperactivated compared to baseline at the 24 hour time point. The most likely explanation for this is that reactivation of the pathway occurred following the loss of negative feedback when pERK was briefly suppressed by **14** at earlier time points. However, it may also be possible that either lower concentrations of **14** or its slow dissociation rate could be contributing to the pathway hyperactivation. Dose-dependent modulation of pMEK, DUSP6, and SPRY4 were similar to those described for pERK (data not shown).[23]

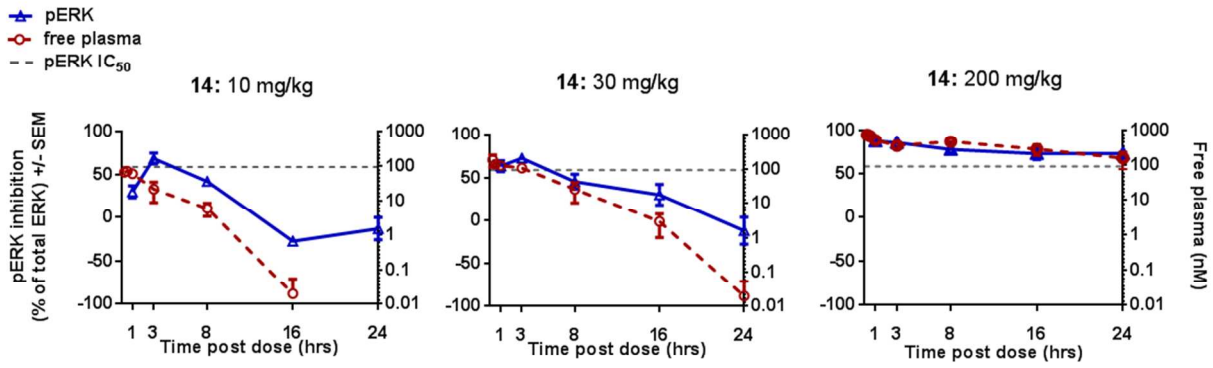

Figure 7. PK/PD analysis of 14 in the human Calu-6 NSCLC xenograft in mice. Percent pERK inhibition (left axis), and free exposure (right axis) following a single dose of **14**, at time points indicated, in Calu-6 tumor bearing mice

Efficacy and tolerability of 14 in the Calu-6 xenograft model. The antitumor efficacy and tolerability of **14** were determined in the Calu-6 xenograft nude mouse model. Mice were treated with vehicle or **14** at 10, 30, or 200 mg/kg p.o. daily beginning 12 days after tumor implantation and continued until day 27. The anti-tumor activity was determined by assessing %T/C or % regression on day 27 post-implant (15 days of treatment). Treatment with **14** resulted in dose-dependent anti-tumor activity with 10 mg/kg being

sub-efficacious (%T/C = 92%), 30 mg/kg resulted in measurable anti-tumor activity (%T/C=46%) and 200 mg/kg resulted in mean tumor regression of 92%, while the same high dose was not efficacious in the PC3, KRAS WT model (Supporting Information Figure 1A). All doses were well tolerated with no significant body weight loss and no signs of toxicity or mortalities were observed (Figure 8 and Supplementary Figure 1B).

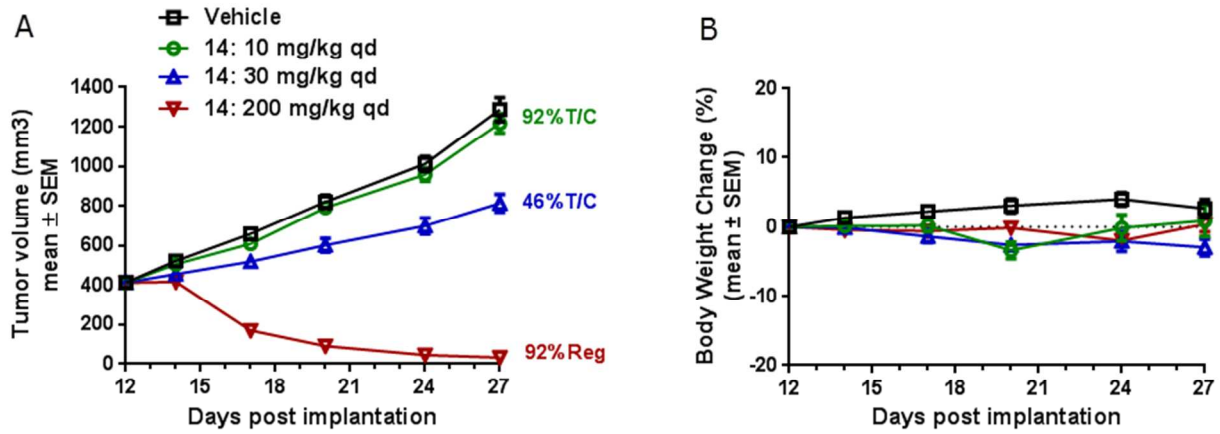

Figure 8. Efficacy of **14** in Calu-6 xenograft in mice. Tumor volumes (A) or percent body weight change from initial (B) treatment groups vs. vehicle control.

Chemistry: Compounds from Tables 2 and 3 were synthesized according to Schemes 1, 2 and 3. The synthesis of morpholine-core bromide moieties are illustrated in Scheme 1. Starting with commercially available **15**, formation of the morpholine was obtained by reaction with 1-bromo-2-(2-bromoethoxy)ethane in the presence of DIEA at 120 °C to provide product **16** in 70% yield (Scheme 1). By reacting **16** with HCl in dioxane at reflux the corresponding pyridone was obtained which upon treatment with K_2CO_3 and iodomethane an approximately 5:1 ratio of the N-alkylated and O-alkylated products (**17** and **16**) was obtained and easily separable by column chromatography.

The pyrazinone bromide **19** was synthesized by starting with commercially available bis-bromide **18** and treating with morpholine at 100 °C. Upon isolation of the product (**19**) N-methylation was accomplished as described above to give a major isomer as the desired product **20**.

Bromide **22** was synthesized by starting with **21** and utilizing the procedure for the ring closure of the morpholine as described above for the synthesis of **16** to give intermediate **22** in 76% yield.

Scheme 1. Synthesis of core/morpholine bromides

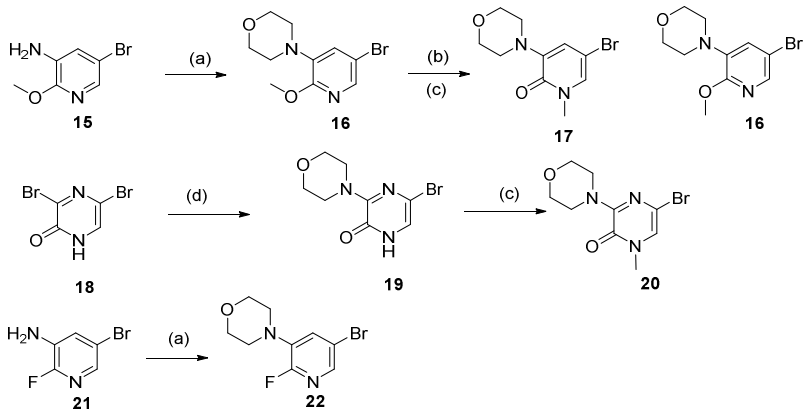

Reagents and Conditions. (a) 1-bromo-2-(2-bromoethoxy)ethane, DMF, DIEA, 120 °C, 70-76%; (b) HCl, dioxane, 110 °C, 93%; (c) K_2CO_3, DMF, MeI, 76-91%; (d) Morpholine, 100 °C, 61%.

Intermediates containing the central phenyl or central pyridine and induced fit motifs were synthesized according to Scheme 2. Starting with **23**, reaction with 3-(trifluoromethyl)benzoyl chloride in DCM and DIEA afforded intermediate **24**. Upon borylation of **24**, boronic ester intermediate **25** was isolated in 71% yield. Compound **28** was obtained by treating the commercially available bromide **26** with bis(pinacolato)diboron, KOAc and Pd(dppf)Cl_2-DCM in dioxane to give boronate ester **27**. Reduction of the nitro functionality to the corresponding aniline **28** was accomplished with hydrogen and Pd/C in 99% yield. Boronate ester **30** was easily prepared by reacting **29** with 3-(trifluoromethyl)benzoyl chloride in DCM and DIEA.

Scheme 2. Synthesis of boronic ester intermediates

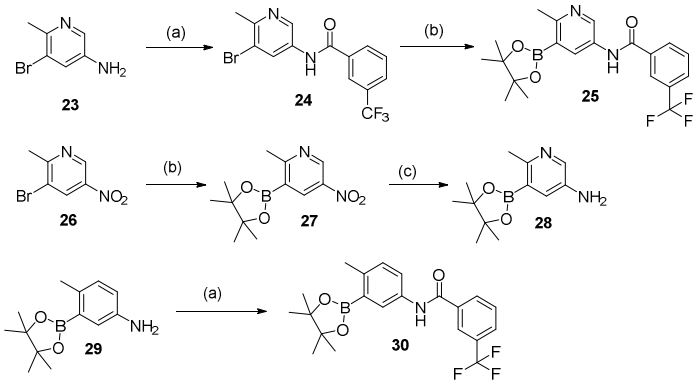

Reagents and Conditions. (a) ArCOCl, DCM, DIEA, 96-100%; (b) Pd(dppf)Cl_2-DCM, dioxane, bis-(pinacolato)diboron, KOAc, 70-80%; (c) H_2, Pd/C, 99%.

Final compounds (**7**, **8**, **9** and **10**) were obtained by the Suzuki-Miyaura reaction between the core bromides and the appropriate boronic esters as illustrated in Scheme 3. Alternatively, final compounds were also obtained via a Suzuki-Miyaura reaction with the core bromides and the boronic ester **28**, followed by amide bond formation with the appropriate carboxylic acid in the presence of EDC and HOAt.

In order to enable last step diversification and obtain final compounds exemplified in Table 3, intermediate **31** was synthesized via Suzuki-Miyaura coupling reaction between **22** and **25**. Treatment of this intermediate with the desired pre-formed alkoxide in THF allowed for isolation of final products (**12**, **13**, and **14**) upon HPLC purification (Scheme 3).

Scheme 3. Final compounds synthesis

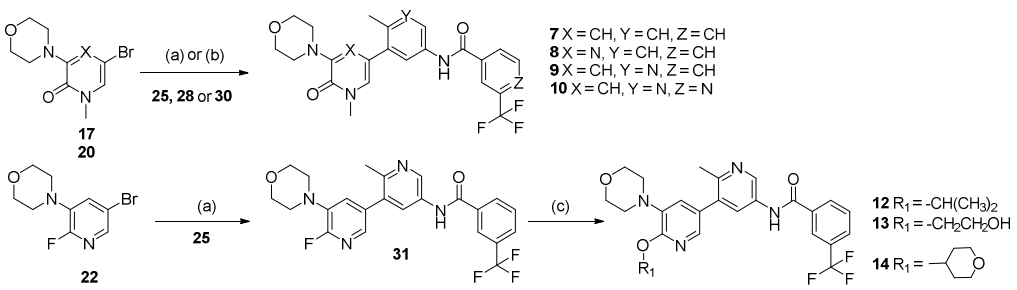

Reagents and Conditions. (a) Pd(dppf)Cl_2-DCM, DME, 2M Na_2CO_3, 120 °C; (b) Pd(dppf)Cl_2-DCM, DME, 2M Na_2CO_3, 120 °C, boronic ester, then DMF, EDC, HOAt, carboxylic acid; (c) R_1-OH, NaH, Dioxane or DMF, 80-105 °C.

CONCLUSION: Despite the clinical activity of RAF and MEK inhibitors in $BRAF^{V600}$ mutant melanoma, they are relatively ineffective in RAS mutant tumors, leaving a significant unmet medical need. The class of RAF inhibitors approved for the treatment of $BRAF^{V600mut}$ melanoma, including vemurafenib and dabrafenib, induce paradoxical activation in BRAF wild-type cells and can induce growth of RAS^{mut} tumors. However, given the central role of CRAF in driving mutant KRAS-driven tumorigenesis, there remains a significant interest in developing RAF inhibitors that will be efficacious in RAS mutant tumors. Our work demonstrates that type 2 RAF inhibitors have the potential to be effective in RAS mutant tumors because they induce minimal paradoxical activation compared to RAF inhibitors with other binding modes (i.e. type 1 or type 1.5). However, previous type 2 RAF inhibitors have suffered from a lack of selectivity, potency and solubility. We set out to address these key issues in the design of a next-generation type 2 RAF inhibitor and in this manuscript we describe the discovery of **14**. By considering saturation as a characteristic to modulate kinase selectivity during hit selection we identified our starting point, a morpholine analog **3** which demonstrated good selectivity. A strategy focused on lowering lipophilicity to address solubility enabled the identification of **7,** a potent type 2 RAF inhibitor in KRAS mutant tumor cells with minimal paradoxical activation. Limitations associated with solubility and formulation of **7** and challenges in balancing physicochemical properties with cellular potency directed the effort towards increasing the Fsp^3 character as a strategy to improve solubility by disrupting crystal packing. This approach led to the identification of **14**, a compound shown to be highly kinase selective and cellularly potent in a KRAS mutant cell line (Calu-6) with minimal paradoxical activation which we believe would enable the compound to be combined with other known linear and/or lateral pathway inhibitors. *In-vivo* evaluation of **14** indicated, it has a reasonable rodent PK profile suitable for PK/PD/efficacy and tolerability studies. **14** was shown to modulate pERK/pMEK[24] *in-vivo* and it

demonstrated dose-dependent tumor regressions in the KRAS mutant Calu-6 xenograft model with no significant body weight loss.

EXPERIMENTAL SECTION

General Methods. The compounds and/or intermediates were characterized by high performance liquid chromatography (HPLC) using a Waters Millennium chromatography system with a 2695 separation module (Milford, MA). The analytical columns were Alltima C-18 reversed phase, 4.6 mm x 50 mm, flow 2.5 mL/min, from Alltech (Deerfield, IL). A gradient elution was used, typically starting with 5% acetonitrile/95% water and progressing to 100% acetonitrile over a period of 10 min. All solvents contained 0.1% trifluoroacetic acid (TFA). Compounds were detected by ultraviolet light (UV) absorption at either 220 or 254 nm. HPLC solvents were from Burdick and Jackson (Muskegan, MI) or Fisher Scientific (Pittsburgh, PA). Mass spectrometric analysis was performed on an LCMS instrument: a Waters system (Alliance HT HPLC and a Micromass ZQ mass spectrometer, Eclipse XDB-C18, 2.1 mm x 50 mm; solvent system, 5-95% acetonitrile in water with 0.1% TFA; flow rate 0.8 mL/min; molecular weight range 200-800; cone voltage 20 V; column temperature 40 °C). All masses were reported as those of the protonated parent ions. ^{1}H nuclear magnetic resonance (NMR) analyses described herein were performed on some of the compounds with a Varian 400-MR MHz NMR (Palo Alto, CA) spectrometer operating at a frequency of 399.89 MHz for ^{1}H or Bruker DRX-500 NMR spectrometer operating at a frequency of 500.13 MHz for ^{1}H. The spectral reference was either TMS or the known chemical shift of the solvent. The spectra were recorded at a temperature of 298 K. Preparative separations were carried out using a Teledyne ISCO chromatography system, or by HPLC using a Waters 2767 sample manager, C-18 reversed phase column, 30 x 50 mm, flow 75 mL/min. Typical solvents employed for the Teledyne ISCO chromatography system and were dichloromethane, methanol, ethyl acetate, and heptane. Typical solvents employed for the reverse phase HPLC were varying concentrations of acetonitrile and water with 0.1% trifluoroacetic acid. The purity of all compounds screened in the biological assays was examined by

LC-MS analysis and were found to be ≥95%. Experimental details for the synthesis and characterization of compounds **3** and **4** are described in the supporting information.

General Procedure for the Suzuki-Miyaura reaction. To the appropriate heteroaryl halide (0.10 mmol) and the appropriate boronic ester (0.12 mmol) in DME (1 mL) was added $PdCl_2$ (dppf).CH_2Cl_2 adduct (0.010 mmol) and 2M aqueous sodium carbonate (0.50 mmol). The reaction mixture was irradiated at 120 °C in a Biotage Initiator microwave for 10-12 min. The cooled reaction mixture was diluted with 2:1 DCM:MeOH (15 mL) and filtered. The filtrate was concentrated and purified by reverse phase HPLC to give the desired product as its TFA salt.

The following compounds were prepared by the above method starting from the appropriate halide and boronic ester.

N-(4-methyl-3-(6-morpholinopyrimidin-4-yl)phenyl)-3-(trifluoromethyl)benzamide (5). Obtained in 51% yield. LCMS (*m/z*) (M+H) = 443.3, Rt = 0.75 min. ^{1}H NMR (500 MHz, DMSO-*d*6) δ ppm 10.70 (s, 1H) 8.86 (s, 1H) 8.26 – 8.38 (m, 2H) 7.93 – 8.06 (m, 2H) 7.74 – 7.90 (m, 2H) 7.43 (d, *J* = 8.5 Hz, 1H) 7.22 (s, 1H) 3.89 (s, 4H) 3.64 – 3.79 (m, 4H) 2.33 (s, 3H) ^{13}C NMR (126 MHz, DMSO-*d*6) δ 164.52, 161.50, 153.48, 137.38, 135.90, 132.32, 131.93, 131.66, 130.32, 129.83, 129.57, 128.82, 125.51, 124.66, 124.63, 123.35, 122.87, 121.72, 103.55, 66.15, 45.40,19.42. HRMS m/z (M^++ 1) calcd 443.1695, obsd 443.1694.

N-(4-methyl-3-(2-morpholinopyridin-4-yl)phenyl)-3-(trifluoromethyl)benzamide (6). Obtained in 28% yield as a white solid. LCMS (*m/z*) (M+H) = 442.3, Rt = 0.76 min. ^{1}H NMR (400 MHz, DMSO-*d6*) δ ppm 10.40 - 10.61 (m, 1 H) 8.30 (s, 1 H) 8.26 (d, *J*=7.83 Hz, 1 H) 8.17 (d, *J*=5.48 Hz, 1 H) 7.90 - 8.03 (m, 1 H) 7.67 - 7.82 (m, 3 H) 7.27 - 7.41 (m, 1H) 7.00 (s, 1 H) 6.82 (d, *J*=5.48 Hz, 1 H) 3.44 - 3.59 (m, 8 H) 2.25 (s, 3 H) . ^{13}C NMR (126 MHz, DMSO-*d*6) δ 164.39, 139.29, 137.33, 136.06, 132.28, 131.37, 130.74, 130.25, 130.22, 129.78, 129.53, 128.69, 125.52, 124.64, 123.35, 121.36, 121.14, 114.59, 109.70, 66.08, 45.95, 19.83. HRMS m/z (M^+ + 1) calcd 442.1742, obsd 442.1742.

N-(4-methyl-3-(1-methyl-5-morpholino-6-oxo-1,6-dihydropyridin-3-yl)phenyl)-3-(trifluoromethyl)benzamide (**7**). Obtained in 15% yield as an off-white solid. LCMS (*m/z*) (M+H) = 472.3, Rt = 0.88 min. ^{1}H NMR (400 MHz, CD_3OD) δ ppm 8.27 (s, 1H), 8.22 (d, *J*=8.2 Hz, 1H), 7.91 (d, *J* =7.8 Hz, 1H), 7.71 - 7.79 (m, 1H), 7.56 - 7.66 (m, 2H), 7.36 (d, *J* =1.6 Hz, 1H), 7.31 (d, *J* =8.2 Hz, 1H), 6.93 (d, *J* =2.0 Hz, 1H), 3.82 - 3.92 (m, 4H), 3.65 (s, 3H), 3.09 - 3.19 (m, 4H), 2.32 (s, 3H). ^{13}C NMR (126 MHz, DMSO-*d*6) δ 164.28, 157.93, 140.77, 138.05, 137.20, 136.17, 132.27, 131.49, 131.10, 130.64, 130.23, 129.77, 129.52, 128.60, 125.54, 124.60, 123.38, 122.06, 121.93, 119.95, 118.61, 66.60, 49.38,37.66, 20.16. HRMS m/z (M^+ + 1) calcd 472.1848, obsd 472.1844.

N-(4-methyl-3-(4-methyl-6-morpholino-5-oxo-4,5-dihydropyrazin-2-yl)phenyl)-3-(trifluoromethyl)benzamide (8). Obtained in 13% yield as a solid. LCMS *m/z* (M+H) = 473.1, Rt = 0.92 min. ^{1}H NMR (400 MHz, CD_3OD) δ ppm 8.25 (s, 1 H) 8.20 (d, *J*=7.83 Hz, 1 H) 7.89 (d, *J*=7.83 Hz, 1 H) 7.67 - 7.80 (m, 2 H) 7.56 (dd, *J*=8.22, 2.35 Hz, 1 H) 7.26 (d, *J*=8.22 Hz, 1 H) 7.18 (s, 1 H) 3.80 (s, 8 H) 3.56 (s, 3 H) 2.39 (s, 3 H) . HRMS m/z (M^+ + 1) calcd 473.1801, obsd 473.1801.

N-(1',2-dimethyl-5'-morpholino-6'-oxo-1',6'-dihydro-[3,3'-bipyridin]-5-yl)-3-(trifluoromethyl)benzamide (9). Obtained in 22% yield as a solid. LCMS *m/z* (M+H) = 473.0, Rt = 0.56 min. ^{1}H NMR (400 MHz, CD_3OD) δ ppm 8.77 (d, J=2.35 Hz, 1 H), 8.29 (s, 1 H), 8.23 (d, J=7.83 Hz, 1 H), 8.12 (d, J=2.35 Hz, 1 H), 7.92 (d, J=8.22 Hz, 1 H), 7.68 - 7.80 (m, 1 H), 7.43 (d, J=2.35 Hz, 1 H), 6.93 (d, J=2.35 Hz, 1 H), 3.77 - 3.94 (m, 4 H), 3.64 (s, 3 H), 3.07 - 3.20 (m, 4 H), 2.52 (s, 3 H). ^{13}C NMR (126 MHz, DMSO-*d*6) δ 164.70, 157.97, 151.42, 141.01, 140.49, 135.61, 133.84, 132.72, 132.35, 131.10, 130.34, 129.06, 124.70, 121.43, 116.76, 66.56, 49.34, 37.71, 23.21. HRMS m/z (M^+ + 1) calcd 473.1801, obsd 473.1804. m.p: 242 °C

N-(1',2-dimethyl-5'-morpholino-6'-oxo-1',6'-dihydro-[3,3'-bipyridin]-5-yl)-2-(trifluoromethyl)isonicotinamide (10). To 5-bromo-1-methyl-3-morpholinopyridin-2(1H)-one (546 mg, 2.0 mmol) and 6-methyl-5-(4,4,5,5-tetramethyl-1,3,2-dioxaborolan-2-yl)pyridin-3-amine (492 mg, 2.1

mmol) in DME (Volume: 11 mL) was added $PdCl_2$ (dppf).CH_2Cl_2 adduct (163 mg, 0.2 mmol) and 2M aqueous sodium carbonate (3.00 mL, 6 mmol). The reaction mixture was irradiated at 125 °C for 20 min. LC-MS showed primarily conversion to product. The cooled reaction mixture was diluted with 2:1 DCM:MeOH (15 mL) and filtered. The filtrate was concentrated with silica gel and purified by flash chromatography over silica gel (ethyl acetate with 0 to 15% methanol gradient) to give 5'-amino-1,2'-dimethyl-5-morpholino-[3,3'-bipyridin]-6(1H)-one (450 mg, 1.498 mmol, 74.9 % yield) as a brown solid. LCMS *m/z* [M + H^+] = 301.0. To a solution of 2-(trifluoromethyl)pyridine-4-carboxylic acid (0.021 g, 0.110 mmol), HOAt (0.015 g, 0.110 mmol), and EDC.HCl (0.021 g, 0.110 mmol) in DMF (0.5 mL) was added 5'-amino-1,2'-dimethyl-5-morpholino-[3,3'-bipyridin]-6(1H)-one (0.030 g, 0.100 mmol). The mixture was stirred overnight at ambient temperature. The reaction mixture was diluted with DMSO, filtered, and purified by HPLC. The clean fractions were lyophilized to give N-(1',2-dimethyl-5'-morpholino-6'-oxo-1',6'-dihydro-[3,3'-bipyridin]-5-yl)-2-(trifluoromethyl)isonicotinamide (13 mg, 0.022 mmol, 21.93 % yield) as a light yellow solid. LCMS (*m/z*) (M+H) = 474.0, Rt = 0.55 min. ^{1}H NMR (400 MHz, CD_3OD) δ ppm 9.23 (d, *J*=2.35 Hz, 1 H) 8.99 (d, *J*=5.14 Hz, 1 H) 8.43 (d, *J*=2.35 Hz, 1 H) 8.37 (s, 1 H) 8.19 (dd, *J*=5.01, 1.54 Hz, 1 H) 7.54 (d, *J*=2.25 Hz, 1 H) 6.97 (d, *J*=2.30 Hz, 1 H) 3.83 - 3.91 (m, 4 H) 3.67 (s, 3 H) 3.14 - 3.22 (m, 4 H) 2.72 (s, 3 H) HRMS m/z (M^+ + 1) calcd 474.1753, obsd 474.1755.

N-(6'-methoxy-2-methyl-5'-morpholino-[3,3'-bipyridin]-5-yl)-3-(trifluoromethyl)benzamide (11). Obtained in 28% yield as a light yellow solid by following the general procedure for the Suzuki-Miyaura reaction. LCMS *m/z* [M + H^+] = 473.3, Rt = 0.73 min. ^{1}H NMR (400 MHz, CD_3OD) δ ppm 9.32 (d, *J*=2.4 Hz, 1H), 8.43 (d, *J*=2.4 Hz, 1H), 8.34 (s, 1H), 8.28 (d, *J*=8.2 Hz, 1H), 7.96 (d, *J*=7.8 Hz, 1H), 7.88 (d, *J*=2.0 Hz, 1H), 7.78 (t, *J*=7.8 Hz, 1H), 7.31 (d, *J*=2.0 Hz, 1H), 4.05 (s, 3H), 3.80 - 3.91 (m, 4H), 3.09 - 3.18 (m, 4H), 2.67 (s, 3H). HRMS m/z (M^+ + 1) calcd 473.1801, obsd 473.1801.

General procedure for S_NAr: To a mixture of sodium hydride, 60% in mineral oil (3.0-5.2 mmol) in 1,4-dioxane or DMF (7 mL) at ambient temperature was added the appropriate alcohol (3.0-5.0 mmol). The mixture was stirred for 15-30 min. N-(6'-fluoro-2-methyl-5'-morpholino-[3,3'-bipyridin]-5-yl)-3-

(trifluoromethyl)benzamide (1.0 mmol) was added, and the reaction was stirred at 80-105 °C for 1-4 hr. The cooled reaction mixture was poured into water (50 mL) and extracted with EtOAc (2x50 mL). The combined organics were washed with brine (25 mL), dried over sodium sulfate, filtered, and concentrated onto silica gel. The mixture was purified by flash chromatography (24 g silica gel, DCM with a 0-10% MeOH gradient over 20 min). Pure product fractions were concentrated to give the desired product. The products could be purified further by reverse phase HPLC or recrystallization from acetonitrile.

The following compounds were prepared by the above method starting from the appropriate alcohol.

N-(6'-isopropoxy-2-methyl-5'-morpholino-[3,3'-bipyridin]-5-yl)-3-(trifluoromethyl)benzamide trifluoroacetic acid salt (12). Obtained in 56% yield as an off-white solid. LCMS *m/z* [M + H^+] = 501.1, Rt = 0.87 min. ^{1}H NMR (400 MHz, DMSO-*d6*) δ ppm 10.92 (s, 1H), 9.03 (s, 1H), 8.33 (s, 1H), 8.21 - 8.31 (m, 2H), 8.02 (d, J=7.8 Hz, 1H), 7.78 - 7.86 (m, 2H), 7.24 (d, J=2.0 Hz, 1H), 5.35 (dt, J=12.2, 6.2 Hz, 1H), 3.67 - 3.78 (m, 4H), 3.06 (m, 4H), 2.52 - 2.56 (s, 3H), 1.34 (d, J=6.3 Hz, 6H). ^{13}C NMR (126 MHz, DMSO-d_6) δ 164.99, 159.01, 158.72, 155.56, 149.30, 138.29, 135.95, 135.72, 135.31, 135.03, 133.37, 132.48, 130.51, 129.96, 129.70, 129.33, 126.64, 125.56, 125.45, 124.82, 123.28, 68.51, 66.54,50.27, 22.41, 20.85. HRMS m/z (M^+ + 1) calcd 501.2114, obsd 501.212. m.p: 204 °C

N-(6'-(2-hydroxyethoxy)-2-methyl-5'-morpholino-[3,3'-bipyridin]-5-yl)-3-(trifluoromethyl)benzamide (13). Obtained in 60% yield as a white solid. LCMS *m/z* [M + H^+] = 503.2, Rt = 0.66 min. ^{1}H NMR (400 MHz, $CDCl_3$) δ ppm 8.63 (d, *J*=2.4 Hz, 1H), 8.13 - 8.19 (m, 2H), 8.09 (d, *J*=7.8 Hz, 1H), 7.95 (br. s., 1H), 7.85 (d, *J*=7.8 Hz, 1H), 7.76 (d, *J*=1.6 Hz, 1H), 7.67 (t, *J*=7.8 Hz, 1H), 7.11 (d, *J*=2.0 Hz, 1H), 4.59 - 4.67 (m, 2H), 3.97 - 4.06 (m, 2H), 3.85 - 3.95 (m, 4H), 3.11 - 3.20 (m, 4H), 2.52 (s, 3H). HRMS m/z (M+ + 1) calcd 503.1906, obsd 503.1907.

N-(2-methyl-5'-morpholino-6'-((tetrahydro-2H-pyran-4-yl)oxy)-[3,3'-bipyridin]-5-yl)-3-(trifluoromethyl)benzamide (**14**). Obtained in 66% yield as an off-white solid. LCMS *m/z* [M + H^+] = 543.1, Rt = 0.77 min. ^{1}H NMR (400 MHz, $CDCl_3$) δ ppm 8.62 (s, 1H), 8.16 (br. s., 2H), 8.10 (d, *J*=7.8

Hz, 1H), 7.86 (d, *J*=7.8 Hz, 2H), 7.77 (d, *J*=2.0 Hz, 1H), 7.63 - 7.73 (m, 1H), 7.07 (d, *J*=2.4 Hz, 1H), 5.43 (dt, *J*=8.1, 4.0 Hz, 1H), 3.95 - 4.06 (m, 2H), 3.83 - 3.94 (m, 4H), 3.70 (ddd, *J*=11.5, 8.4, 3.1 Hz, 2H), 3.10 - 3.25 (m, 4H), 2.54 (s, 3H), 2.17 (dt, *J*=8.7, 4.5 Hz, 2H), 1.89 (dtd, *J*=12.8, 8.49, 8.5, 3.9 Hz, 2H). ^{13}C NMR (126 MHz, DMSO-d_6) δ 164.73, 154.68, 151.28, 140.72, 138.01, 135.84, 133.88, 133.20, 132.37, 130.33, 129.84, 129.59, 129.07, 128.89, 125.89, 125.51, 124.74, 123.34, 69.80, 66.64, 65.03, 50.40,32.19,23.22. HRMS m/z (M^+ + 1) calcd 543.2219, obsd 543.2218. m.p: 196 °C

4-(5-Bromo-2-methoxypyridin-3-yl)morpholine (16). To a solution of 5-bromo-2-methoxypyridin-3-amine (3.00 g, 14.8 mmol, 1.00 equiv) in DMF (40 mL) was added 1-bromo-2-(2-bromoethoxy)ethane (4.11 g, 17.7 mmol, 1.20 equiv.) and DIEA (7.74 mL, 44.3 mmol, 3.00 equiv.). The reaction mixture was stirred at 120 °C for 24 h. Upon cooling to room temperature, the reaction was partitioned between water and EtOAc, the aqueous phase was extracted three times with EtOAc, the organics were combined, dried over Na_2SO_4, filtered and concentrated. The crude material was purified via silica gel flash chromatography eluting with heptanes and ethyl acetate (0-20%) to give 4-(5-bromo-2-methoxypyridin-3-yl)morpholine (2.80 g, 70% yield). LCMS *m/z* [M + H^+] = 273.0/275.0. ^{1}H NMR (400 MHz, $CDCl_3$) δ ppm 7.84 (d, *J*=2.0 Hz, 1H), 7.14 (d, *J*=2.0 Hz, 1H), 3.97 (s, 3H), 3.76 - 3.91 (m, 4H), 2.90 - 3.18 (m, 4H).

5-bromo-1-methyl-3-morpholinopyridin-2(1H)-one (17). A 0.3 M solution of 4-(5-bromo-2-methoxypyridin-3-yl)morpholine (2.5 g, 9.15 mmol, 1.00 equiv.) in 4 M HCl in dioxane (3.8 mL, 45.8 mmol, 5 equiv.) was heated to 100 °C for 1 hr. Upon cooling to room temperature, the reaction was concentrated to dryness under low pressure. The residue was suspended in water (20 mL) and neutralized with solid sodium bicarbonate. The solid was filtered, rinsed with water (2x10 mL) and dried to give 5-bromo-3-morpholinopyridin-2-ol in 93% yield (2.2 g). LCMS *m/z* [M + H^+] = 258.9/260.9. To a 0.3 M solution of 5-bromo-3-morpholinopyridin-2-ol (500 mg, 1.9 mmol, 1.00 equiv.) in DMF (7 mL) was added K_2CO_3 (560 mg, 4.1 mmol, 2.10 equiv.) and iodomethane (0.139 mL, 2.2 mmol, 1.1 equiv.). The reaction mixture was stirred at ambient temperature overnight. LC-MS showed conversion to pyridone

product and about 15-20% of O-alkylated by-product. The reaction mixture was diluted with ethyl acetate and filtered. The filtrate was concentrated under reduced pressure with silica gel. The crude mixture was purified by flash chromatography eluting with heptanes and ethyl acetate (50-100%, then 10:1 ethyl acetate:methanol gradient) to give 5-bromo-1-methyl-3-morpholinopyridin-2(1H)-one (400 mg, 76% yield). LCMS *m/z* [M + H^+] = 272.8/274.9. ^{1}H NMR (400 MHz, $CDCl_3$) δ ppm 7.11 (d, *J*=2.4 Hz, 1H), 6.64 (d, *J*=2.4 Hz, 1H), 3.76 - 3.97 (m, 4H), 3.52 (s, 3H), 3.05 - 3.27 (m, 4H).

5-bromo-3-morpholinopyrazin-2(1H)-one (**19**). A solution of 3,5-dibromopyrazin-2-ol (500 mg, 1.97 mmol, 1.0 equiv.) was heated in morpholine (0.9 mL, 9.85 mmol, 5 equiv.) at 100 °C for 18 hours. Upon overnight stirring, cooled to room temperature and filtered the precipitate. The filtrate was partitioned between water and ethyl acetate, the organic phase was dried with sodium sulfate, filtered and concentrated. The yellow solid was used without further purification (310 mg). LCMS *m/z* [M + H^+] = 259.9/261.9.

5-bromo-1-methyl-3-morpholinopyrazin-2(1H)-one (20). To a solution of 5-bromo-3-morpholinopyrazin-2(1H)-one (22 mg, 0.085 mmol, 1.0 equiv.) in DMF (1 mL, 0.085 M) at 0 °C was added potassium carbonate (23 mg, 0.169 mmol, 2.0 equiv.), followed by iodomethane (0.005 mL, 0.085 mmol, 1.0 equiv.). The reaction was allowed to warm to room temperature and stirred for 2 hours. Partitioned between ethyl acetate and water, the organic phase was dried with sodium sulfate, filtered and concentrated to dryness to give 5-bromo-1-methyl-3-morpholinopyrazin-2(1H)-one in 91% yield as a major isomer. LCMS *m/z* [M + H^+] = 274.0/276.0. ^{1}H NMR (400 MHz, $CDCl_3$) δ ppm 6.77 (s, 1 H) 3.85 - 4.00 (m, 4 H) 3.66 - 3.83 (m, 4 H) 3.42 (s, 3 H).

4-(5-Bromo-2-fluoropyridin-3-yl)morpholine (22). To a stirred solution of 3-amino-5-bromo-2-fluoropyridine (10.0 g, 52.5 mmol, 1.00 equiv) in DMF (100 mL) at 0 °C was slowly added NaH (3.78 g, 157 mmol, 3.00 equiv). The mixture was allowed to warm to room temperature over 15 min and treated with bis(2-bromoethyl) ether (9.89 mL, 79.0 mmol, 1.50 equiv). The mixture was heated to 80 °C and stirred for 3 h. The cooled reaction mixture was poured into water (500 mL) and stirred for 20 min. The

mixture was filtered. The filter cake was washed with water (2 x 50 mL), allowed to air dry for a few hours, and then washed with heptane (2 x 50 mL). The resulting solid was dried to give **20** (10.5 g, 76.4 % yield) as a light brown solid which was used without further purification. LCMS *m/z* [M + H^+] = 261.0/263.0. ^{1}H NMR (400 MHz, $CDCl_3$) δ ppm 7.81 (t, *J*=2.0 Hz, 1H), 7.32 (dd, *J*=9.0, 2.0 Hz, 1H), 3.84 - 3.91 (m, 4H) , 3.11 - 3.16 (m, 4H).

N-(5-bromo-6-methylpyridin-3-yl)-3-(trifluoromethyl)benzamide (24). To a solution of 3-bromo-2-methylpyridin-5-amine (510 mg, 2.73 mmol, 1.00 equiv) in DCM (10 mL) was added DIEA (0.476 mL, 2.73 mmol, 1.00 equiv) and 3-(trifluoromethyl)benzoyl chloride (569 mg, 2.73 mmol, 1.00 equiv.). The mixture was stirred at ambient temperature for 2 h. The reaction mixture was washed sequentially with water (10 mL) and brine (10 mL), dried over sodium sulfate, filtered, and concentrated to give N-(5-bromo-6-methylpyridin-3-yl)-3-(trifluoromethyl)benzamide (980 mg, 100 % yield) as an off-white solid which was used without further purification. LCMS *m/z* [M + H^+] = 359.0/361.0. ^{1}H NMR (400 MHz, DMSO-*d6*) δ ppm 10.70 (m, 1H), 8.78 (m, 1H), 8.46 (m, 1H), 8.28 (m, 2H), 7.98 (m, 1H), 7.78 (m, 1H), 2.55 (m, 3H).

N-(6-methyl-5-(4,4,5,5-tetramethyl-1,3,2-dioxaborolan-2-yl)pyridin-3-yl)-3-(trifluoromethyl)benzamide (25). To a solution of N-(5-bromo-6-methylpyridin-3-yl)-3-(trifluoromethyl)benzamide (10.5 g, 29.2 mmol, 1.00 equiv) in 1,4-dioxane (9 mL) was added bis(pinacolato)diboron (11.1 g, 43.9 mmol, 1.50 equiv), potassium acetate (5.74 g, 58.5 mmol, 2.00 equiv) and $PdCl_2$(dppf).CH_2Cl_2 adduct (2.39 g, 2.92 mmol, 0.100 equiv). The reaction was stirred at reflux for 2 h. The cooled reaction mixture was diluted with ethyl acetate (20 mL) and filtered through Celite. The filtrate was concentrated and purified by flash chromatography over silica gel (220 g, heptanes with 0-100% ethyl acetate gradient) to give N-(6-methyl-5-(4,4,5,5-tetramethyl-1,3,2-dioxaborolan-2-yl)pyridin-3-yl)-3-(trifluoromethyl)benzamide (6.69 g, 70.7% yield) as an off-white solid.

LCMS *m/z* [M + H^+] = 325.0. ^{1}H NMR (400 MHz, DMSO-*d6*) δ ppm 10.43 - 10.60 (m, 1H), 8.88 - 9.01 (m, 1H), 8.22 - 8.42 (m, 3H), 7.90 - 8.05 (m, 1H), 7.68 - 7.84 (m, 1H), 2.53 - 2.65 (m, 3H), 1.31 (s, 12H).

2-methyl-5-nitro-3-(4,4,5,5-tetramethyl-1,3,2-dioxaborolan-2-yl)pyridine (27). To a degassed mixture of 3-bromo-2-methyl-5-nitropyridine (12.67 g, 58.4 mmol, 1.0 equiv.), bis(pinacolato)diboron (17.79 g, 70.1 mmol, 1.2 equiv.), and KOAc (17.19 g, 175 mmol, 3.0 equiv.) in Dioxane (Volume: 160 mL) was added $PdCl_2$(dppf).CH_2Cl_2 adduct (2.384 g, 2.92 mmol, 0.05 equiv.). The resulting mixture was stirred at 100 °C for 3 hrs. The cooled mixture was diluted with ethyl acetate and filtered through Celite. The filtrate was adsorbed onto Celite and purified by flash chromatography (heptanes with 0-20% ethyl acetate gradient). The clean fractions were concentrated to give 2-methyl-5-nitro-3-(4,4,5,5-tetramethyl-1,3,2-dioxaborolan-2-yl)pyridine (12.7 g, 48.1 mmol, 82 % yield) as a white solid. ^{1}H NMR (400 MHz, $CDCl_3$) δ ppm 9.33 (d, *J*=2.74 Hz, 1 H) 8.79 (d, *J*=2.74 Hz, 1 H) 2.87 (s, 3 H) 1.39 (s, 12 H).

6-methyl-5-(4,4,5,5-tetramethyl-1,3,2-dioxaborolan-2-yl)pyridin-3-amine (28). A degassed solution of 2-methyl-5-nitro-3-(4,4,5,5-tetramethyl-1,3,2-dioxaborolan-2-yl)pyridine (12.7 g, 48.1 mmol) in MeOH (Volume: 160 mL) was treated with 10% palladium on carbon (Degussa type) (0.614 g, 0.577 mmol). The mixture was purged and flushed with hydrogen three times and stirred under a hydrogen balloon overnight at ambient temperature for 17 hours. The degassed mixture was filtered through Celite. The filter cake was rinsed with additional methanol. The combined filtrates were concentrated and then dried under high vacuum to give 6-methyl-5-(4,4,5,5-tetramethyl-1,3,2-dioxaborolan-2-yl)pyridin-3-amine (11.1 g, 47.4 mmol, 99 % yield) as an off white solid. ^{1}H NMR (400 MHz, $CDCl_3$) δ ppm 8.05 (d, *J*=3.13 Hz, 1 H) 7.38 (d, *J*=3.13 Hz, 1 H) 2.63 (s, 3 H) 1.35 (s, 12 H)

N-(4-methyl-3-(4,4,5,5-tetramethyl-1,3,2-dioxaborolan-2-yl)phenyl)-3-(trifluoromethyl)benzamide (30). To a solution of 4-methyl-3-(4,4,5,5-tetramethyl-1,3,2-dioxaborolan-2-yl)aniline (7.59 g, 32.6 mmol, 1.0 equiv.) in THF (300 mL, 0.1 M) at 0 °C was added 3-trifluoromethylbenzoylchloride (4.8 mL, 32.6 mmol, 1.0 equiv.) and the reaction

mixture was brought to room temperature. After 3 hours, the reaction was concentrated under low pressure and dried under vacuum to give 12.6 g of the desired product in 96% yield. LCMS *m/z* [M + H^+] = 406.2, Rt = 1.24 min.

N-(6'-Fluoro-2-methyl-5'-morpholino-[3,3'-bipyridin]-5-yl)-3-(trifluoromethyl)benzamide (31). To a solution of 4-(5-bromo-2-fluoropyridin-3-yl)morpholine (4.65 g, 16.03 mmol) and N-(6-methyl-5-(4,4,5,5-tetramethyl-1,3,2-dioxaborolan-2-yl)pyridin-3-yl)-3-(trifluoromethyl)benzamide (7.81 g, 19.23 mmol) in DME (90 mL) was added 2M aqueous sodium carbonate (24.04 mL, 48.1 mmol). Argon was bubbled through the mixture for 5 min. $PdCl_2$(dppf).CH_2Cl_2 adduct (0.785 g, 0.962 mmol) was added, and the mixture was purged with argon briefly, fitted with an air-cooled condenser, and then heated at 100 °C for 1.5 hr. The cooled reaction mixture was poured into water (80 mL) and extracted with EtOAc (2 x 120 mL). The combined organics were washed with brine (50 mL), dried over sodium sulfate, filtered, and concentrated with silica gel. The mixture was purified by flash chromatography (120 g silica gel, DCM with 0-10% MeOH gradient). Product fractions were concentrated to give N-(6'-Fluoro-2-methyl-5'-morpholino-[3,3'-bipyridin]-5-yl)-3-(trifluoromethyl)benzamide (6.38 g, 77.7 % yield) as a beige solid. LCMS *m/z* [M + H^+] = 461.2. 1H NMR (400 MHz, DMSO-*d6*) δ ppm 10.67 (s, 1H), 8.87 (d, *J*=2.4 Hz, 1H), 8.31 (s, 1H), 8.27 (d, *J*=7.8 Hz, 1H), 8.06 (d, *J*=2.4 Hz, 1H), 7.98 (d, *J*=7.8 Hz, 1H), 7.73 - 7.87 (m, 2H), 7.52 (dd, *J*=10.2, 2.0 Hz, 1H), 3.65 - 3.83 (m, 4H), 3.03 - 3.16 (m, 4H), 2.41 (s, 3H).

Data mining. We created a tailored knowledgebase, drawing from historical RAF biochemical IC_{50}s (all isoforms, mutant and wildtype) and cellular EC_{50}s (target modulation or cell proliferation) from assays using cells driven by mutant RAF or mutant RAS. Compounds were selected for this knowledgebase if they had scored at least one IC_{50} or EC_{50} value < 10 uM in one of the historical assays. The knowledgebase of 28k compounds was further annotated with scaffold information, comprised of both substructure matches from scaffolds as defined by medicinal chemists in the historical programs as well as canonical level03 and level04 scaffolds as determined by the scaffold tree algorithm.[24] The substructure-based scaffolds were used to categorize compounds as type 1, type 2 or type 1.5 inhibitors

whereas the scaffold tree scaffolds were used in the selection protocols to ensure coverage of available chemotypes. Subset selection was a combination of cheminformatics protocols and chemistry review to focus on chemical matter with historical potency (especially in target modulation assays), SAR tractability (small series, not singletons) and physical chemical properties. The cRAF biochemical assay was a filter for entry into the activation assay (requiring < 1 uM IC_{50}) resulting in a dataset of around 200 compounds with cRAF IC_{50} and cellular data; a 116 compound subset had a pMEK EC_{50} <= 0.3 uM which made them suitable for assessing activation.

Biochemical Assay

The CRAF kinase assay was carried out using 10 nM kinase-dead MEK1 protein substrate (carrying a K97R mutation), 3 μM ATP, and 10 pM CRAF Y340E/Y341E. The reaction buffer contained 50 mM Tris pH 7.5, 10 mM $MgCl_2$, 0.05% BSA, 50 mM NaCl, 0.01% Tween-20 and 1 mM DTT. The reactions were carried out at room temperature in a volume of 10 μL in white 384-shallow well plates (PorxiPlate, Perkin Elmer, Waltham , MA) for 40 min and stopped by adding 5 μL/well quench solution (50 mM Tris pH 7.5, 50 mM EDTA). Terminated reactions received 5 μL/well detection reagents consisting of 50 mM Tris pH7.5, 0.01% Tween-20, 1:1000 diluted anti-phospho MEK1/2 S217/S221 antibody (Cell Signaling Technology, Danvers, MA), 0.01 mg/mL each of AlphaScreen Protein A-coated acceptor beads and streptavidin-coated donor beads (PerkinElmer). Plates were read in an EnVision plate reader (PerkinElmer) after overnight incubation at room temperature. In compound inhibition studies, compounds were tested over a concentration range of 25 μM to 1.74E-6 μM in 16-point, 3 fold format. DMSO was at a final concentration of 0.5%. Compounds were pre-incubated with CRAF for 30 min before adding substrates to start the reaction. Inhibition data were fit to a four parameter logistic equation to calculate the IC_{50} of the compounds **3-14**

Biochemical Kinase Specificity Profile of 7.

The kinase specificity profile for compound 7 reported in Figure 7 was determined as previously described.[25] Compound 7 was assessed in the DiscoverX KINOME*scan* binding assay at 1 μM with activity presented as % of control = [(test compound signal − positive control signal)/(negative control signal − positive control signal]] × 100. Data for the 457 kinase KINOME*scan* are in Supporting Information.

***In vivo* PK/PD and efficacy**

Mouse studies were undertaken in accordance with the Novartis Institutes for Biomedical Research Animal Care and Use Committee protocols and regulations. Mice were housed in a temperature- and humidity-controlled animal facility with *ad libitum* access to food and water and acclimated for at least 3 days before experimental procedures.

For tumor PD measurements in the Calu-6 model, tumor bearing mice were randomized into treatment groups and treated with vehicle or a single oral administration of 14 at 10, 30, or 200 mg/kg. Tumor samples were collected at 1, 3, 8, 16, and 24 hrs post single dose of 14 (n=3/time point) and analyzed for levels of phosphorylated ERK1/2 (Thr202/Tyr204; Thr185/Tyr187) and total ERK using the MesoScale Discovery (MSD) platform. Briefly, the pulverized tumor was lysed in Tris lysis buffer (supplied by MesoScale Discovery Multi-Spot assay system), and centrifuged at 11,000 rpm for 20 min. (4°C). Supernatants were collected for protein lysates. Relative amounts of phosphorylated and total ERK were determined using the Multi-Spot Assay System K151CWD-2 and K151DUD-2 from MSD. Plasma samples were collected at 0.25, 0.5, 1, 3, 8, 16, and 24 post single dose of 14 (n=3/time point) and concentrations of 14 were measured by LC-MS.

For efficacy in Calu6 xenograft tumors, $10x10^6$ Calu-6 cells in 50% Matrigel™ were implanted subcutaneously into the right flank of female nude mice (6-8 weeks old). Mice were randomized into treatment groups on day 12 post implantation, when the average tumor volume was ~400 mm^3. Mice were grouped (n=8) and treated with vehicle (20% Captisol) or 14 at 10, 30, or 200 mg/kg qd.

Treatments began on day 12 and continued until day 27 post implantation. Tumor volume and body weights were collected at the time of randomization and twice per week for the study duration. Tumor volume was determined by measurement with calipers and calculated using a modified ellipsoid formula, where tumor volume (TV) (mm^3) = [((l x w2) x 3.14159)) / 6], where l is the longest axis of the tumor and w is perpendicular to l. Mice were monitored for tumor growth, body weight and body condition. Animal well-being and behavior were monitored twice weekly. General health of mice was monitored daily.

Crystallization of Wild-Type BRAF

The kinase domain of wild-type BRAF (residues 445-723) was expressed using the baculovirus-expression system, purified by Ni-NTA chromatography, and concentrated to 2 mg/mL in a buffer composed of 20 mM Bis-Tris propane pH 7.0, 15% glycerol, and 1 mM TCEP plus 0.1% CHAPS. Crystals with wild-type BRAF were grown by the vapor diffusion method at 291K in hanging drops. Crystals were grown at 18 ˚C by mixing equal volumes of protein incubated with 0.3 mM of an internal control compound and the following well solution: 100 mM Tris pH 8.4, 100 mM NaCl, and 12% PEG8000. The internal control compound was then displaced by soaking the crystal overnight in cryosolution of 100 mM Tris pH 8.4, 15% PEG8000 and 20% glycerol supplemented with 300 μM of the desired target compound. However, co-crystals can also be obtained by complexing wild-type BRAF protein directly with the target compound and performing co-crystallization experiments as described above.

Data processing and refinement

Data were collected at beam-lines 5.0.1 and 5.0.2 of the Advanced Light Source at Lawrence Berkeley National Laboratory (Berkeley, CA) and processed with autoPROC.[26] Structures were solved by molecular replacement using the 5CT7 BRAF structure as search model in PHASER[27] and refined with BUSTER.[28] All models were built with COOT.[29]

Small molecule crystal structure. Single crystals of **7** suitable for X-ray structural investigation were obtained from a methanol solution by slowly evaporating the solvents. Diffraction data were collected at 100 K on a Bruker AXS MicroStar diffractometer using a SMART 6000 CCD detector on a three-circle platform goniometer with Cu(K_α) radiation (λ= 1.54178 Å) from a microfocus rotating generator equipped with Incoatec multilayer optics (Helios confocal mirror system). 16 ω-scans at different ϕ-positions were performed to ensure appropriate data redundancy (11.1, Friedel pairs merged).

Collected images were processed using SAINT software (SAINT V7.36A, Bruker AXS 2006). Scaling and absorption correction (multi-scan method) of the raw data were performed with program SADABS (SADABS V2008/1, Sheldrick G.M. 2008). The semi-empirical absorption correction is based on the intensities of symmetry-related reflections measured at different angular settings (minimum and maximum transmission 0.931 and 0.973; ratio of minimum to maximum transmission is 0.957). Assignment of space group and setup of files for structure solution was done using program XPREP (XPREP V2008/2, Sheldrick G.M. 2008).

The structure was solved by dual-space recycling methods and refined on F^2 with the SHELXTL suite of programs (SHELXTL V6.12, Sheldrick G.M. 2001). Anisotropic displacement parameters were used for all non-hydrogen atoms. Hydrogen atoms were unambiguously located in difference Fourier maps and refined in idealized positions using rigid methyl or hydroxyl groups or a riding model. The structure consists of two independent molecules. In molecule 2, all numbers used for molecule 1 have been increased by 40. Data are deposited under CCDC 1508642.

Final data: $C_{25}H_{24}F_3N_3O_3$, M_r = 471.47, crystal size 0.08x0.06x0.03 mm^3 (grown from methanol), monoclinic, space group $P2_1/n$ (No. 14) with a = 16.334 (3), b = 13.727 (3), c = 21.539(4) Å, β = 108.839(11)°, V = 4570.7(16) $Å^3$, Z = 8, D_c = 1.370 $g.cm^{-3}$, μ = 0.908 mm^{-1}, F(000) = 1968, 94814 reflections measured, 8382 independent, R_{int} = 0.0508, 2.98° < θ < 68.22°, T = 100(2) K, 617 parameters,

R_1 = 0.0354, wR_2 = 0.0846 for 8382 reflections with $I > 2\sigma(I)$, R_1 = 0.0452, wR_2 = 0.0910 for all 8382 data, GoF = 1.034, restrained GoF = 1.034, res. el.dens. = +0.30/-0.34 e·Å^{-3}.

SUPPORTING INFORMATION

The Supporting Information is available free of charge on the

Cellular assay conditions, Compound **7** data for the 457 kinase KINOME*scan*, X-ray data table for **3** and **14,** extended data for the small molecule crystal structure **7**, PC3 xenograft study data with experimental details, and machine-readable representation of structures with key data (CSV).

AUTHOR INFORMATION

Corresponding Author

*E-mail: Savithri.ramurthy@novartis.com. Telephone: **510-879-9463**

ORCID

Savithri Ramurthy: 0000-0002-2444-5309

Notes

The authors declare no competing financial interest.

ACKNOWLEDGEMENTS

We thank Dazhi Tang, Elaine Ginn, Colin Lorentzen, Kent Wong and Linda Xiao for generating solubility, in vitro ADME data as well as Shengtian Yang for running NMR structural elucidation of **14**.

ABBREVIATIONS USED

Fsp^3, fraction sp^3; Sol, solubility; CP, cell proliferation; Cl, clearance; Vss, volume of distribution; DIEA, diisopropylethylamine; EDC, 1-ethyl-3-(3-dimethylaminopropyl)carbodiimide; HOAt, 1-hydroxy-7-

azabenzotriazole; SNAr, nucleophilic aromatic substitution; Rt, retention time; TCEP, (Tris(2-carbosyethyl) phosphine)

REFERENCES

(1) Aversa, R.A.; Barsanti. P.A.; Burger, M.; Dillon, M.P.; Dipsea, A.; Hu, C.; Lou, Y.; Nishiguchi, G.; Pan, Y.; Polyakov, V.; Ramurthy, S.; Rico, A.; Setti, L.; Smith, Aaron.; Subramanian, S.; Taft, B.; Tanner, H.; Wan, L.; Yusuff, N. Biaryl amide compounds as kinase inhibitors and their preparation. WO 2014151616

(2) Ostrem, J. M.; Peters, U.; Sos, M.L.; Wells, J.A.; Shokat, K.M. K-Ras(G12C) inhibitors allosterically control GTP affinity and effector interactions. *Nature* **2013**, *503*(7477), 548-551.

(3) Lito, P.; Solomon, M.; Li, L.S.; Hansen, R.; Rosen, N. Allele-specific inhibitors inactivate mutant KRAS G12C by a trapping mechanism. *Science* **2016**, *351*(6273), 604-608.

(4) Patricelli, M.P.; Janes, M.R.; Li, L.S.; Hansen, R.; Peters, U.; Kessler, L.V.; Chen, Y.; Kucharski, J.M.; Feng, J.; Ely, T.; Chen, J.H.; Firdaus, S.J.; Babbar, A.; Ren, P.; Liu, Y. Selective inhibition of oncogenic KRAS output with small molecules targeting the inactive state. *Cancer Discov*. **2016** Mar;*6*(3), 316-329.

(5) Karreth, F.A.; Frese, K.K.; DeNicola, G.M.; Baccarini, M.; Tuveson, D.A. C-Raf is required for the initiation of lung cancer by K-Ras (G12D) *Cancer Discov.* **2011**, Jul;*1*(2), 128-136.

(6) Blasco, R. B.; Francoz, S.; Santamaria, D.; Canamero, M.; Dubus, P.; Charron, J.; Baccarini, M.; Barbacid, M. C-Raf, but not B-Raf, is essential for development of K-Ras oncogene-driven on-small cell lung carcinoma. *Cancer Cell* **2011**, May 17; *19*(5), 652-663.

(7) Caunt, C.J.; Sale, M.J.; Smith, P.D.; Cook, S.J. MEK1 and MEK2 inhibitors and cancer therapy: the long and winding road. *Nat. Rev. Cancer* **2015** Oct; *15*(10), 577-592.

(8) Joseph E.W.; Pratilas, C.A.; Poulikakos, P.I.; Tadi, M.; Wang, W.; Taylor, B.S.; Halilovic, E.; Persaud, Y.; Xing, F.; Viale A.; Tsai, J.; Chapman, P.B.; Bollag, G.; Solit, D.B.; Rosen, N. The RAF

inhibitor PLX4032 inhibits ERK signaling and tumor cell proliferation in a V600E BRAF-selective manner. *Proc. Natl. Acad. Sci USA* **2010**, Aug 17; *107*(33), 14903-14908.

(9) Hatzivassiliou, G.; Song, K.; Yen, I.; Brandhuber, B.J.; Anderson, D.J.; Alvarado, R.; Ludlam, M.J.; Stokoe, D.; Gloor, S.L.; Vigers, G.; Morales, T.; Aliagas, I.; Liu, B.; Sideris, S.; Hoeflich, K.P.; Jaiswal, B.S.; Seshagiri, S.; Koeppen, H.; Belvin, M.; Friedman, L.S.; Malek, S. RAF inhibitors prime wild-type RAF to activate the MAPK pathway and enhance growth. *Nature* **2010**, Mar 18; *464*(7287), 431-435.

(10) Heidorn, S.J.; Milagre, C.; Whittaker, S.; Nourry, A.; Niculescu-Duvas, I.; Dhomen, N.; Hussain, J.; Reis-Filho, J.S.; Springer, C.J.; Pritchard, C.; Marais, R. Kinase-dead BRAF and oncogenic RAS cooperate to drive tumor progression through CRAF. *Cell* **2010**, Jan 22; *140* (2), 209-221.

(11) Lito, P.; Saborowski, A.; Yue, J.; Solomon, M.; Joseph, E.; Gadal, S.; Saborowski, M.; Kastenhuber, E.; Fellmann, C.; Ohara, K.; Morikami, K.; Miura, T.; Lukacs, C.; Ishii, N.; Lowe, S.; Rosen, N. Disruption of CRAF-mediated MEK activation is required for effective MEK inhibition in KRAS mutant tumours. *Cancer Cell* **2014** May 12; *25*(5), 697-710.

(12) Lamba, S.; Russo, M; Sun, C.; Lazzari, L.; Cancelliere, C.; Grernrum, W.; Lieftink, C.; Bernards, R.; DiNicolantonio, F.; Bardelli, A. RAF suppression synergizes with MEK inhibition in KRAS mutant cancer cells. *Cell Rep*. **2014**, Sep 11; *8*(5), 1475-1483

(13) Peng, S.B.; Henry J.R.; Kaufman, M.D.; Lu, W.P.; Smith, B.D.; Vogeti, S.; Rutkoski, T.J.; Wise, S.; Chun, L.; Zhang.; Van Horn, R.D.; Yin, T.; Zhang, X.; Yadav, V.; Chen, S.H.; Gong, X.; Ma, X.; Webster, Y.; Buchanan, S.; Mochalkin, I.; Huber, L.; Kays, L.; Donoho, G.P.; Walgren, J.; McCann, D.; Patel, P.; Conti, I.; Plowman, G.D.; Starling, J.J.; Flynn, D.L. Inhibition of RAF isoforms and active dimers by LY3009120 leads to anti-tumor activities in RAS or BRAF mutant cancers. *Cancer Cell* **2015**, Sep 14; *28*(3), 384-398.

(14) Fabbro, D. 25 years of small molecular weight kinase inhibitors: potentials and limitations. *Mol. Pharmacol*. **2015**, May; *87*(5), 766-775.

(15) Liu,Y.; Gray, N.S. Rational design of inhibitors that bind to inactive kinase conformations. *Nat. Chem. Biol.* **2006**, *2*, 358-364.

(16) Angiolini, M. Targeting the DFG-in kinase conformation: a new trend emerging from patent analysis. *Future Med. Chem*. **2011**, *3*, 309-337.

(17) Ishikawa, M.; Hashimoto, Y. Improvement in aqueous solubility in small molecule drug discovery programs by disruption of molecular planarity and symmetry. *J. Med. Chem.* **2011**, *54*, 1539-1554.

(18) Lovering, F.; Bikker, J.; Humblet, C. Escape from flatland: increasing saturation as an approach to improving clinical success. *J. Med Chem*. **2009**, *52*, 6752-6756.

(19) Fabian, M. A.; Biggs III, W. H.; Treiber, D. K.; Atteridge, C. E.; Azimioara, M. D.; Benedetti, M. G.; Carter, T. A.; Ciceri, P.; Edeen, P. T.; Floyd, M.; Ford, J. M.; Galvin, M.; Gerlach, J. L.; Grotzfeld, R. M.; Herrgard, S.; Insko, D. E.; Insko, M. A.; Lai, A. G.; Lelias, J-M.; Mehta, S.A.; Milanov, Z. V.; Velasco, A.M.; Wodcka, L.M.; Patel, H.K.; Zarrinkar, P.P.; Lockhart, D.J. A small molecule-kinase interaction map for clinical kinase inhibitors. *Nat. Biotechnol.*, **2005**, *23*, 329-336.

(20) Karaman, M. W.; Herrgard, S.; Treiber, D. K.; Gallant, P.; Atteridge, C. E.; Campbell, B. T.; Chan, K.W.; Ciceri, P.; Davis, M. I.; Edeen, P. T.; Faraoni, R.; Floyd, M.; Hunt, J. P.; Jockhart, D.J.; Milanov, Z. V.; Morrison, M. J.; Pallares, G.; Patel, H.K.; Pritchard, S.; Wodicka, L. M.: Zarrinkar, P. P. A quantitative analysis of kinase inhibitor selectivity. *Nat. Biotechnol.* **2008**, *26*, 127-132.

(21) Vijayan, R.S.K.; He. P.; Modi. V.;Krisna, C.; Duong-Ly.; Ma. H.; Peterson, J.R.; Dunbrack, R.L.; Levy, R.M. Conformational analysis of the DFG-Out kinase motif and biochemical profiling of structurally validated Type II inhibitors. *J. Med Chem*. **2015**, *58*, 466-479.

(22) Experimental detail for the small molecule crystal structure of **7**, and Xray co-crystal structure data table of 3 and 14 and kinase profile of **7** are given in the supporting information

(23) Manuscript discussing the entire biology of **14** has been submitted for publication.

(24) Schuffenhauer, A.; Ertl, P.; Roggo, S.; Wetzel, S.; Koch, M.A., and Waldmann, H. The scaffold tree – visualization of the scaffold universe by hierarchical scaffold classification. *J. Chem Inf. Model* **2007**, *47*, 47-58.

(25) Vonrhein, C.; Flensburg, C.; Keller, P.; Sharff, A.; Smart, O.; Paciorek, W.; Womack, T.; Bricogne, G. Data processing and analysis with the *autoPROC* toolbox. *Acta Crystallogr. D. Biol. Crystallogr.* **2011**, *67*, 293–302.

(26) McCoy, A. J.; Grosse-Kunstleve, R. W.; Adams, P. D.; Winn, M. D.; Storoni, L. C.; Read, R. J. *Phaser* crystallographic software. *J. Appl. Crystallogr.* **2007**, *40*, 658–674.

(27) Smart, O. S.; Womack, T. O.; Flensburg, C.; Keller, P.; Paciorek, W.; Sharff, A.; Vonrhein, C.; Bricogne, G. Exploiting structure similarity in refinement: automated NCS and target-structure restraints in *BUSTER*. *Acta Crystallogr. D. Biol. Crystallogr.* **2012**, *68*, 368–380.

(28) Emsley, P.; Lohkamp, B.; Scott, W. G.; Cowtan, K. Features and development of Coot. *Acta Crystallogr. D. Biol. Crystallogr.* **2010**, *66*, 486–501.

"Table of Contents graphic."

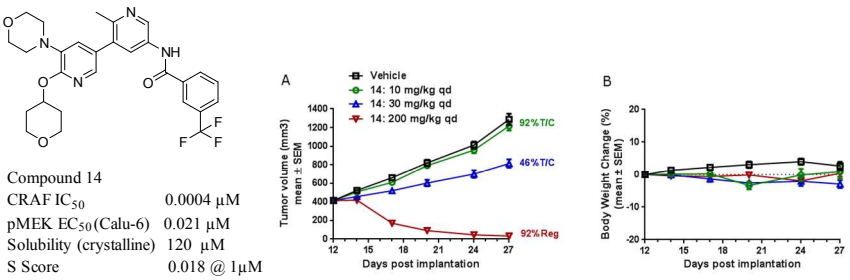

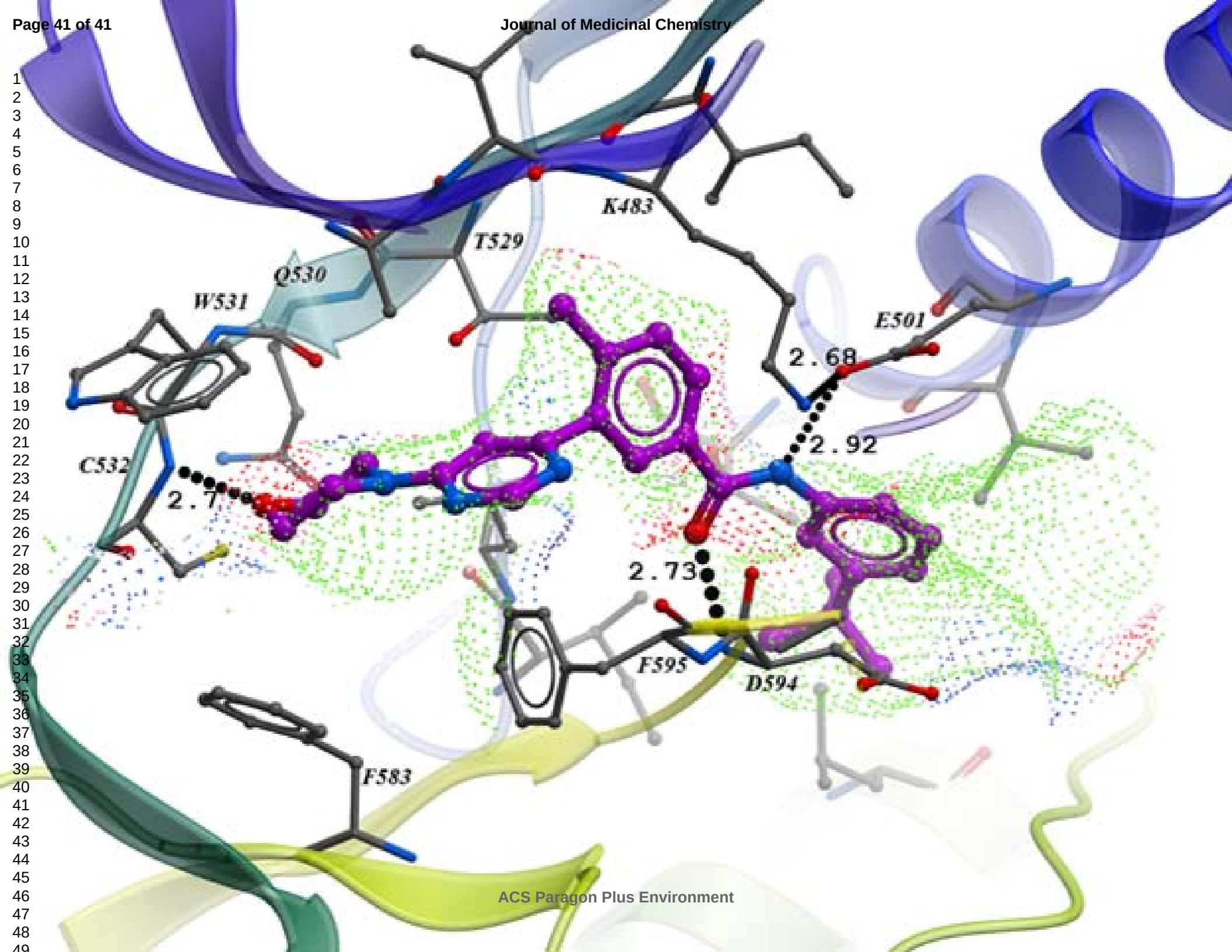
K483
T529
Q530
W531
E501
2.68
2.92
C532
2.7
2.73
F595
D594
F583

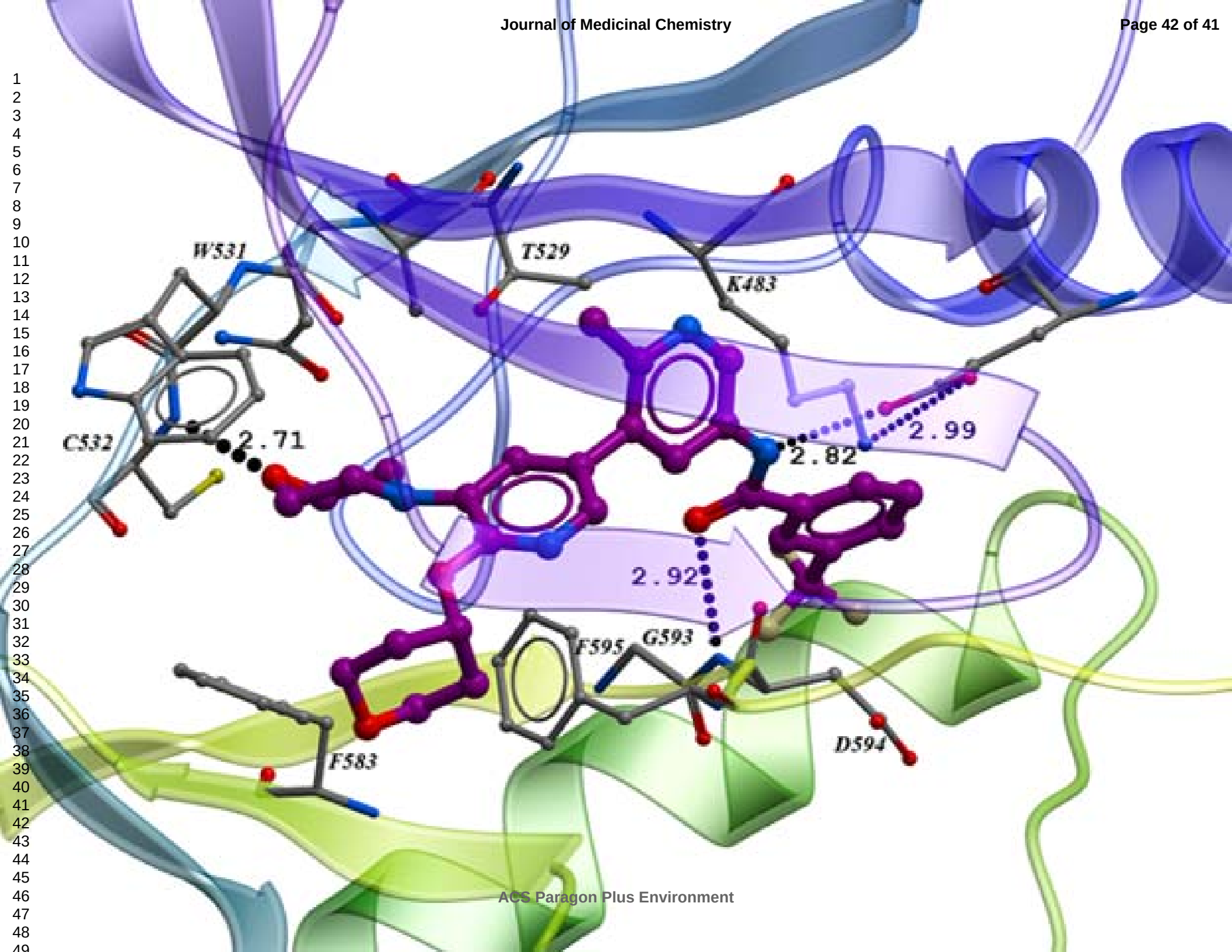
W531
T529
K483
C532
2.71
2.82
2.99
2.92
F595
G593
D594
F583